The Thesis Committee for Leo Young Zeng
Certifies that this is the approved version of the following Thesis:

Seismic-based geomorphology of a mixed carbonate siliciclastic shelf-to-basin submarine drainage system, Miocene, Browse Basin, Northwest Shelf of Australia

APPROVED BY
SUPERVISING COMMITTEE:

Xavier Janson, Supervisor

Charles Kerans

Jake Covault

Seismic-based geomorphology of a mixed carbonate siliciclastic shelf-to-basin submarine drainage system, Miocene, Browse Basin, Northwest Shelf of Australia

by

Leo Young Zeng

Thesis

Presented to the Faculty of the Graduate School of

The University of Texas at Austin

in Partial Fulfillment

of the Requirements

for the Degree of

Master of Science in Geological Sciences

The University of Texas at Austin

August 2020

Acknowledgements

The author would like to acknowledge Equinor for sponsoring this project in the form of a fellowship, the Reservoir Characteristics Research Laboratory (RCRL) of the Bureau of Economic Geology, University of Texas at Austin for providing data and software for this study, and Ellis and Halliburton for generously providing educational licenses of Paleoscan and Openworks software, respectively. The members of the Zeng thesis committee, Charles Kerans and Jacob Covault, are acknowledged for their help in writing and reviewing this paper.

Abstract

Seismic-based geomorphology of a mixed carbonate siliciclastic shelf-to-basin submarine drainage system, Miocene, Browse Basin, Northwest Shelf of Australia

Leo Young Zeng, M.S.Geo.Sci

The University of Texas at Austin, 2020

Supervisor: Xavier Janson

Recent studies revealed that carbonate slopes can have similar architectural elements as their siliciclastic counterparts. This study uses a large regional 3D seismic dataset to map and quantify carbonate and mixed carbonate-siliciclastic slope architectural elements to generate an updated model of these slope systems. The research area of this project is the upper slope to toe-of-slope region of Miocene carbonates in the Browse Basin of the NW Shelf of Australia covering a total of over 25,000 km^2 in area. This slope can be divided into three components: (1) a low angle transition between carbonate platform margins and the upper slope; (2) a steep upper slope riddled with low-sinuosity, line-fed canyons; and (3) a low angle lower slope with a mix of sinuous channel-levee systems, mass transport deposits, and slope fans. The slope channels were sourced from large carbonate platforms along the shelf. Slope architectural elements, such as canyons, channel-levee systems, mass transport deposits, and fans, were imaged to extract geomorphic data such as length, gradient, aspect ratio, and sinuosity. Canyons are defined

as channels between 0.5 to 1.5 km wide and 80 to 250 m deep that are relatively straight (sinuosity of 1.00-1.14) and set upon the steeper gradients of the upper slope (2.4° - 11°). Some canyons transformed downstream into channel-levee systems, which are narrower and shallower and more sinuous (1.05-1.30), developing on a slope angle of 1.2° - 4.6°. In many cases, the evolution of canyons into channel-levee systems can be clearly observed in seismic data in the middle-outer slope. The development of the channel-levee systems in the lower slope is controlled by slope gradient and concavity. The channel-levee system can be eroded by large mass transport deposits. This high-resolution regional 3D seismic dataset provides an excellent example of a carbonate slope to toe-of-slope morphology that can be used to generate an updated model of such systems and provide a new analogue for exploring other carbonate slope and basin environments.

Table of Contents

List of Tables

List of Figures

INTRODUCTION

Recent studies of modern carbonate slopes using high resolution multibeam datasets (Mulder et al. 2012, Principaud et al. 2015, Tournadour et al. 2015, Puga-Bernabeu et al. 2013, Counts et al. 2018) have revealed a more complex morphology than can be found in classic models of carbonate slopes (Cook et al. 1983, Mullins and Cook 1986, Coniglio and Dix 1992). These older models either strongly emphasize the line-sourced apron of unconfined accumulation or apply channel-fan architecture from siliciclastic systems without much evidence to support it. If any channels are shown, they are typically straight without any levees (Payros and Pujalte 2008). Older carbonate slopes revealed by either outcrop or seismic studies also show carbonate slopes without extensive channel and canyons systems on the slopes. Few studies have illustrated levees or channelized slopes in ancient deposits (Phelps and Kerans 2007, Payros et al. 2007).

Studies using multibeam surveys show that modern carbonate slopes have lower slope architecture akin to that of siliciclastic slopes, but the steeper upper and middle slope are dominated by straight or low sinuosity, somewhat regularly spaced, canyons and gullies. In a backscatter survey done over the Little Bahamas Bank (Tournadour et al. 2015), one can see large complex canyons that carry large quantities of sediment out onto the basin floor. In a multibeam survey of the Great Bahamas Bank (Principaud et al. 2015), large gully systems line the entirety of the slope profile, whereas slides and other slope failures generate scars and escarpments on the slope and create mass transport deposits (MTD) in the basin. In another multibeam survey of the Great Barrier Reef (Puga-Bernabeu et al. 2013), deep canyons line the shelf edge and carry sediment well out onto the basin floor where large high backscatter anomalies occur and are interpreted as deep water fans.

However, carbonate slope architectural complexities are not just found in modern slopes. Previous studies using high resolution 3D seismic on Permian, Cretaceous and Neogene carbonate slopes (Janson pers. comm. 2018) have shown similar architecture as modern systems, with extensive canyon systems fueling large sinuous channel-levee systems that funnel sediments downslope into unconfined systems in the deep basin. The recent documentation of extensive channelized systems along the carbonate-dominated continental shelves and large isolated carbonate platforms of various ages seems to suggest that the concept of carbonate slope aprons being fed by unconfined line source systems could be revised. This study focuses on a thick Miocene carbonate and mixed carbonate-siliciclastic slope system in the Northwest Shelf of Australia that would be characterized as a slope apron system, which is defined by extensive debris deposits that develop parallel to adjacent shelf/slope breaks (Mullins and Cook 1986). Using a set of large recent 3D seismic surveys, this study investigates and quantifies the various geomorphologies that can be found along the Miocene carbonate slope and how its architecture differs distinctly from a classic carbonate apron model. The study also aims to understand the change in geomorphology as the slope transition from steep (>5°) to gentle (<3°) gradients and how it relates to regional and local processes on the shelf and slope.

GEOLOGICAL SETTING

The Northwest Shelf of Australia (NWS) is a SW-NE trending passive continental margin located between 12° and 22°S latitude offshore Western Australia and includes a series of sedimentary basins stretching between 100-200 km wide (Fig. 1). The study area is located on the edge of the Browse Basin on its border with the Roebuck Basin to the south. The Browse Basin is a sedimentary depocenter bordered to the west by the Scott Plateau and the east by the Leveque Shelf (Blevin et al. 1998). The Browse Basin is structurally a system of half-grabens dipping towards the continent, a result of rift events caused by the separation of the Greater Indian Plate and western Australian Plate during the Early Permian (Struckmeyer et al. 1998). A contractional reactivation of Paleozoic faults occurred in the Late Triassic to Early Jurassic, resulting in partial inversion of the half-graben, and led to the formation of large-scale anticlinal and synclinal features. Afterwards, a thick sequence of shelf sediments was deposited until the late Oligocene or early Miocene, when renewed tectonic activity caused by the collision of the western Australian plate and the Banda Arc reactivated the old Jurassic fault trends. While these tectonic events largely affected the NWS, they only had a minor influence on the slope or the study region (Fig. 2 and 3).

During this period of tectonic inversion, the NWS developed a series of thick, prograding carbonate units (Stephenson and Cadman, 1994). Apthorpe (1988), Moss et al. (2004), and Collins et al. (2006) observed corals and coral fragments in well cuttings of the Oligocene to Miocene in the study region, with the Apthorpe (1988) study based in the Browse Basin, and the others in the Carnarvon Basin to the South. In total, about 5 sequences of carbonate buildups were observed in the Miocene (Fig. 3A, Belde 2017, Janson pers. comm. 2018). The third carbonate platform buildup, which contributed to the

progradation of the shelf and is the focus of this paper (Fig. 3B), was dated through well cuttings to be of Burdigalian to Tortonian (early to middle Miocene) (Belde et al. 2017).

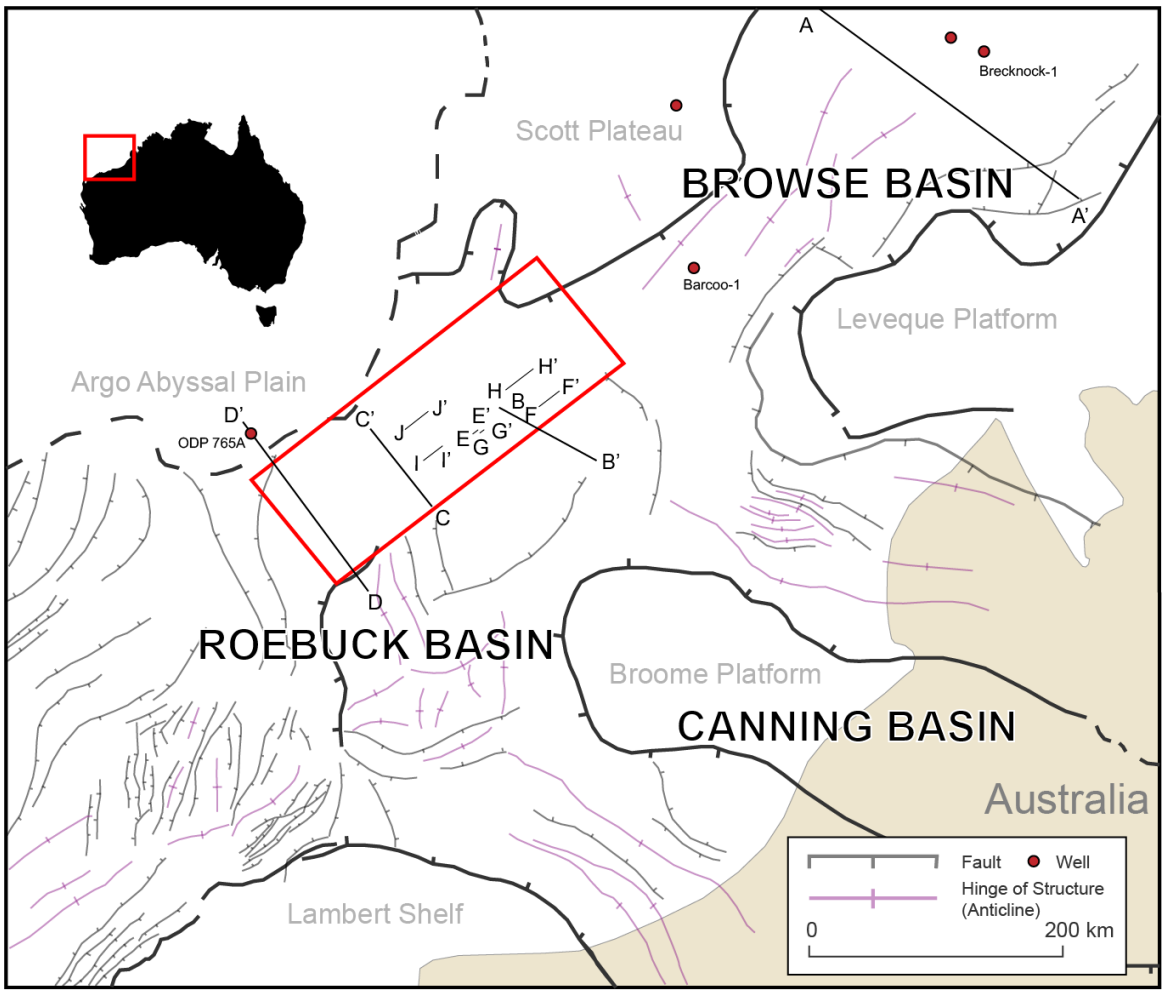

Figure 1: Regional map of the NWS. The study area is outlined in the red box. The study area is relatively free of regional faults and tectonic structures. Positions of seismic sections used in this study are shown. Red dots indicate regional wells with information about lithology and age. Adapted from Geoscience Australia.

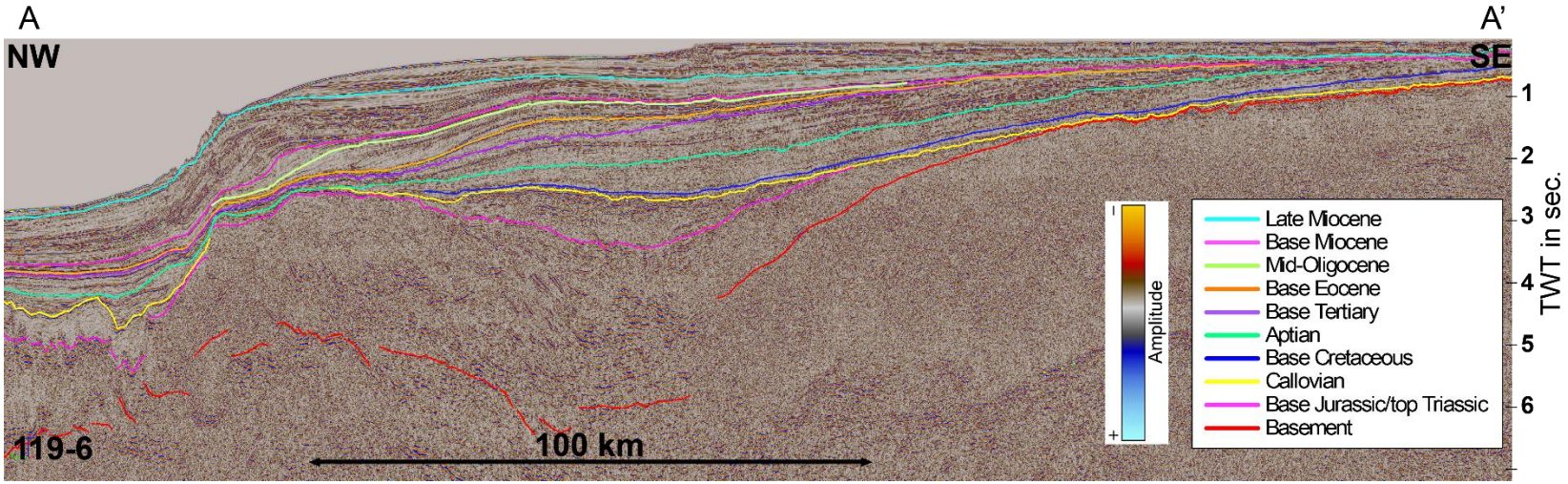

Figure 2: Interpreted regional seismic line of the Browse Basin, showing the inversion structures in the base Jurassic and depositional geometry in the Oligocene to Miocene. See location in Fig. 1.

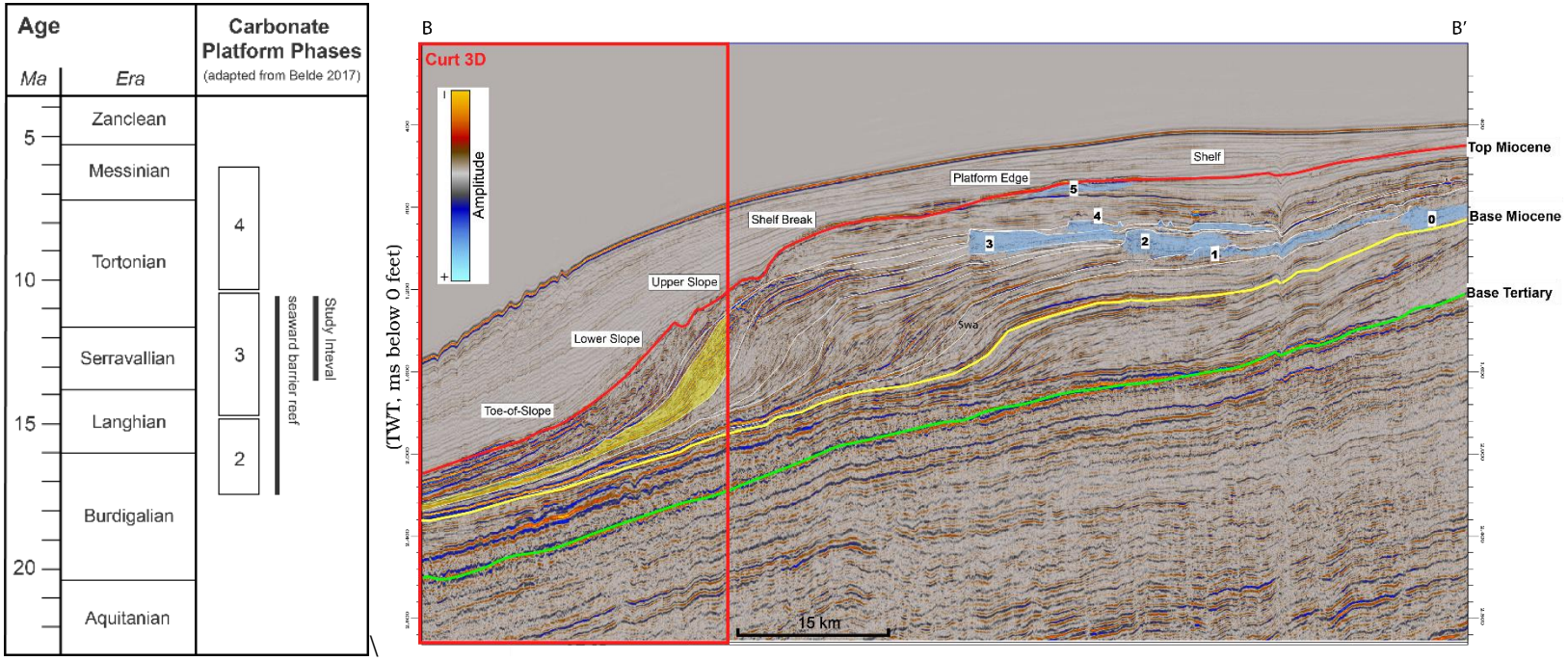

Figure 3: A) Stratigraphic column marking the cycles of carbonate growth in the Miocene in the Browse Basin. Adapted from Belde et al. (2017). B) Regional cross section (B-B') of the Browse Basin. Refer to Fig. 1 for the location in the regional map. The intersection with Curt3D is represented by the red box. The yellow shaded area indicates the study interval. The numbers on the shaded blue areas indicate the carbonate platform cycle as described by Belde et al. (2017). Adapted from Janson pers. comm. (2018)

Belde et al. (2017) studied the platform evolution of the Browse Basin, which is essential to fully understand the patterns of carbonate slope sedimentation in study area. The oldest carbonate build-ups are interpreted as a large bryozoan build-up of Oligocene age (34.03–27.8 Ma). In the late Burdigalian (Fig. 3A), tropical reef growth started, forming an extensive barrier reef (Phase 1, Fig. 3B). From the mid-Langhian to the early Tortonian, the barrier-reef system along margin grew to more than 500 km in length (Phases 2-3, Fig. 3B). After the early Tortonian, the reefs retreated (Phase 4, Fig. 3B), likely as a result of climatic cooling following the Mid-Miocene Climate Optimum in concert with increased subsidence rates. The high subsidence rates in the north promoted the development of thick, aggrading platforms. Lower subsidence in the south, where the study area is located, resulted in thinner, larger platforms. The final growth of reef and platform ended around 6 Ma (Phase 5, Fig. 3B), as the shelf transitioned into one dominated by fine drift sedimentation. Belde et al. (2017) and Rosleff-Soerensen et al. (2016) age dated the carbonate build-ups using primarily sidewall cores of wells in the region. In those studies, strontium dating was the primary method of age dating, although relative age dating was also used.

Very few wells penetrate the Miocene slope in the Browse Basin. Of those wells, some have cuttings and some have wireline logs (mostly gamma ray logs). Both the cuttings and the wireline logs show that the slope is dominated by carbonate sediments (Janson pers. comm. 2018). An analysis of the Ocean Drilling Program (ODP) 765A well by Janson pers. comm. (2018) reveals a thick accumulation of Miocene calciturbidites sourced from the slope (refer to location in Fig. 1 and 7). Since the study region contains part of the slope that feeds into this well, it can be assumed that the calciturbidites found in the well can also be found on the slope. More importantly, a very low percentage (<5%) of siliciclastic material is found in those distal turbidites, and only in the lowermost part of the Miocene

suggesting that there was not any significant siliciclastic input in the system. Cuttings and low gamma-ray values in the Miocene from nearby wells (Fig. 1) also indicate a mostly carbonate-dominated shelf and slope (Janson pers. comm. 2018, Belde et al. 2017), and that there is little sand in the lower Miocene (5-10%), and almost none in the middle Miocene. Regional studies have shown that at one point during the middle Miocene, the carbonate platforms that developed near the shelf edge were developing an almost continuous barrier separating the inner shelf and slope area. A few seaways interrupted this barrier (Janson pers. comm. 2018) in other areas of the Browse Basin. We will consider this slope system as a carbonate-dominated mixed carbonate-siliciclastic system to account for a possible existence of a seaway that interrupts the carbonate platform updip of our seismic coverage, even though additional older vintage 2D seismic lines immediately outside the 3D coverage do not show a large seaway similar to other parts of the Browse Basin (Janson pers. comm. 2018).

DATA

This study uses the Curt 3D seismic survey, acquired at the transition between the Browse Basin and the Roebuck Basin. This high-quality/high-resolution volume covers an area of approximately 25,000 km^2. Due to the large size of the Curt 3D volume, it was divided into four roughly equal-sized subparts – Curt 1, Curt 2, Curt 3, and Curt 4, with Curt 1 as the southwestern-most section, and Curt 4 as the northeastern-most section (Fig. 3). The dominant frequency of the seismic data is 40 hz. Bin size of the 3D survey is 12.5 x 12.5 m. The calculated seismic resolvable limit is 12.5 ms (21.25 m). The vertical range of the study area was limited to a single clinoform in the middle Miocene interval. At the time of this study, there were no well logs within the region that can be used to calibrate a time-depth conversion, but a value of Vp = 3.4 km/s (Calculated from Kronoa-1 well data in the Browse Basin, Tuyl et al. 2018) was used for velocity in carbonates when converting time data to depth.

METHODS

This study aims to quantify the seismic geomorphologic features found throughout the slope in the seismic volume. This study follows traditional siliciclastic slope geomorphic analysis (Posamentier and Kolla 2003) and quantitative seismic geomorphology (Wood 2007). In carbonate slope-to-basin seismic geomorphology, previous studies conducted in other areas of the Australian NWS (Janson pers. comms. 2018, Rosleff-Soerensen et al. 2012) and Permian West Texas (Janson et al. 2007, Kerans et al. 1994) provided valuable analogues.

Seismic geomorphology is a technique that describes depositional landscape (landform) using seismic geometry and attributes (Posamentier and Kolla 2003). Through seismic, the form, origin, evolution, and distribution of these features are interpreted and described assuming that the reflectors follow geological time (Vail et al. 1977, Mitchum et al. 1977). This can be done qualitatively, where the data are predominately observations and human descriptions, or quantitatively, where data collection and manipulation in digital form are used in lieu of nominal descriptions to describe the data. In this study, quantitative measures, such as landform dimension measurements, were employed to generate a dataset of the various slope architectures that were used in data manipulation and visualization.

The interpretation of the slope system was made using a 100-slice horizon-stack through the spectral decomposition volumes using the full-volume 3D seismic interpretation workflow described by Paumard et al. (2019). Horizon surfaces were generated through horizon stacking (Fig. 4). For this technique, the specified volume is thoroughly traced and marked with grid points that follow the seismic reflections. Modeled surfaces are then interpolated from these grid points, generating stacks of surface patches.

This process was done mostly automatically, though it required some manual corrections at the end to finish, including adjusting the grid points and connecting adjacent surface patches. Finally, full horizons are interpreted from these surface patches, creating the horizon stack. The interpretation of the horizon stack depends on the quality and continuity the of surface patches, and minor corrections may be required to ensure the quality and continuity for a usable horizon stack. For each sub-volume, 100 horizons were generated within the study interval. The relatively large number of horizons generated was to ensure a higher resolution of time slices and cleaner connection with adjacent sub-volumes, since the horizon stacks of each sub-volume was generated separately.

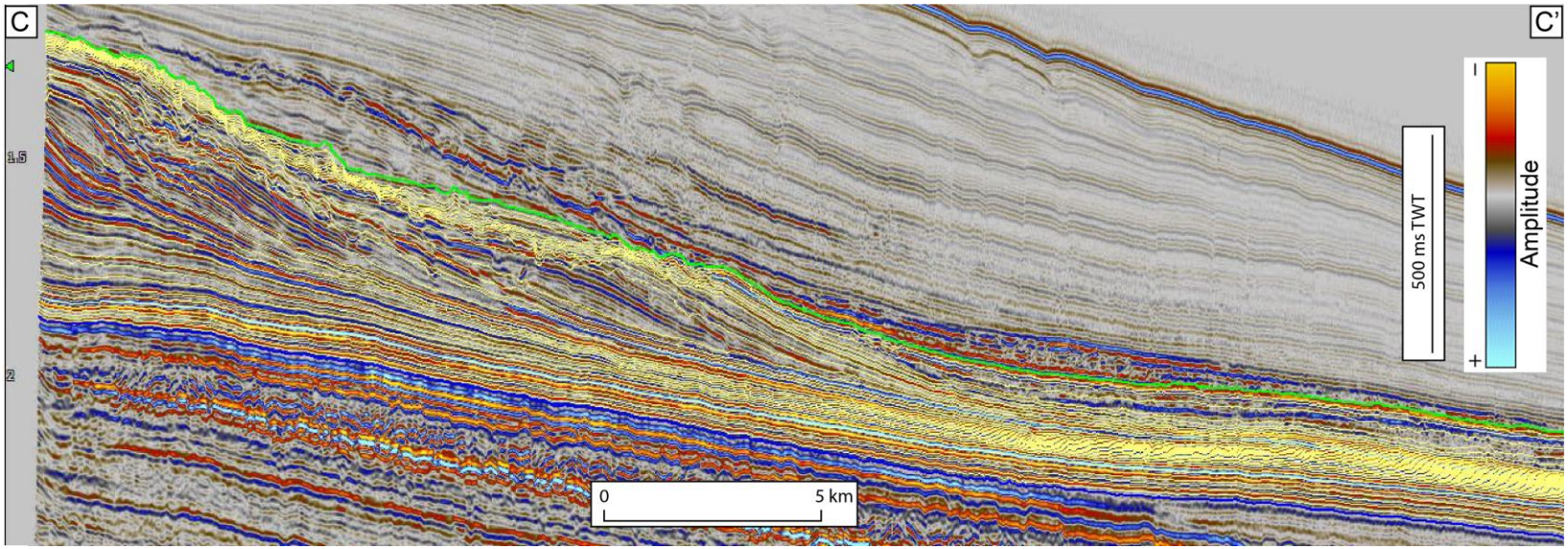

Figure 4: An example of a horizon stack model in the study interval. Horizon stack models were used to quickly generate layered surfaces for convenient viewing. Each yellow line represents a horizon.

Two seismic attributes were used in the geomorphologic analysis of Curt3D, coherency and spectral decomposition. These attributes were mapped onto horizon stacks generated through model gridding. These two attributes, along with the original post-stack seismic volume, were essential to quantifying the various slope architectural elements used in the study.

The coherency attribute (Marfurt et al. 1998), which defines how similar adjacent reflections are to each other, is used to highlight slope architecture such as channels or MTDs. This attribute is generated by measuring the similarity in waveform of the 3D volume, and emphasizes discontinuous events, such as faults or channels. In this study, the coherency attribute volume was primarily viewed through a horizon coherency slice, which offered a clearer picture of the various slope elements than a vertical view.

The second attribute used here is spectral decomposition (Partyka et al. 1999). This attribute filters the seismic volume based on a frequency, which would highlight attributes with a thickness of that frequency. By color blending several frequencies of data, a comprehensive view of a variety of thicknesses represented by different colors can be created. In this study, spectral decomposition was primarily used for identifying fans, because their intervals make it harder to observe through coherency or amplitude. The frequencies used for the color blending are 30 hz, 45 hz, and 60 hz.

One horizon slice was selected to map and quantify the slope architectural elements. This slice was extracted and loaded into GIS software for digitizing. These elements include channels, fans, and MTDs. Channels were traced and their lengths were measured to obtain sinuosity values. Fans were measured for their lengths and widths.

In channels, the digitization was done through multiple measurements of each channel identified on the attribute slices. The length of the channel was extracted by tracing the thalweg throughout the entire channel body. The width was measured by averaging

three cross-sections of the channel, one at the proximal area, one at the distal area, and one in between. Due to the resolution of seismic, it is possible that channel lengths were measured to be shorter than their actual values, and that some of the shallower channels may be overlooked. In total, 108 channels were measured, and their measurement data are recorded in table 1.

Similarly, MTDs and fans were also measured. Their lengths were measured across the widest area of the deposits parallel to the dip of the slope, and their widths are the same but for the strike of the slope. These data are recorded in table 2.

Sinuosity was calculated by dividing the total length of a channel by the straight distance between its start and end. Slope angle was calculated by dividing the vertical distance a channel travels by its length, and then converted into degrees.

Zone	Canyon	CLS	Canyon Length (m)	Canyon Straight Length (km)	Canyon Sinuosity	Canyon Start Z (ms)	Canyon End Z (ms)	CLS Length (m)	CLS Straight Length (km)	CLS Sinuosity	Channel End Z (ms)	Canyon Angle (°)	CLS Angle (°)
1	1		19310	18.6	1.04	1670	2322					3.3	
1	2		6640	6.4	1.03	1589	2061					6.9	
1	3		16140	15.8	1.02	1610	2221					3.7	
1	4		14780	14.3	1.03	1632	2193					3.7	
1	5		15830	15.1	1.05	1319	2193					5.4	
1	6		14910	14.6	1.02	1475	2134					4.3	
1	7	1	13910	13.6	1.02	1531	1890	29520	24.3	1.22	2508	2.5	2.0
1	8	2	9840	9.8	1.01	1375	1988	45350	39.7	1.14	2541	6.0	1.2
1	9	3	6900	6.7	1.04	1387	1811	11660	11.0	1.06	2131	6.0	2.7
1	10		16600	16.6	1.00	1406	2017					3.6	
1	11		14960	14.9	1.00	1427	1966					3.5	
1	12		15980	15.3	1.04	1451	1854					2.5	
1	13		15820	15.4	1.03	1404	1964					3.4	
1	14		24740	22.2	1.11	1282	2004					2.8	
1	15		21020	20.9	1.01	1238	2065					3.8	
1	16		20910	20.3	1.03	1217	2028					3.8	
1	17		15890	15.6	1.02	1246	1924					4.1	
1	18		15240	15.0	1.02	1258	1923					4.2	
1	19		19480	18.7	1.04	1368	2069					3.5	
2	1		14220	14.0	1.01	1537	2039					3.4	
2	2		13050	12.8	1.02	1440	1911					3.5	
2	3		16170	16.0	1.01	1432	2047					3.7	
2	4		14360	14.1	1.01	1431	2020					4.0	
2	5		13740	13.4	1.03	1449	2009					4.0	
2	6		13340	13.1	1.02	1421	1997					4.2	
2	7		17670	17.4	1.01	1375	2036					3.6	
2	8		14870	14.3	1.04	1463	2044					3.8	
2	9	1	9100	8.9	1.02	1418	1817	15680	14.3	1.10	2142	4.3	2.0
2	10		12300	11.9	1.03	1442	1975					4.2	
2	11		12830	12.5	1.02	1355	1956					4.6	
2	12	2	6200	6.0	1.04	1426	1683	5500	5.1	1.08	1908	4.0	4.0
2	13	3	8900	8.2	1.09	1442	1775	12660	12.0	1.06	2120	3.6	2.7
2		4					1775	6230	5.7	1.09	1932		2.5
2		5					1775	6910	6.3	1.09	1936		2.3
2	14	6	4700	4.1	1.14	1372	1583	9930	9.1	1.10	1964	4.4	3.7
2	15	7	7320	7.1	1.03	1369	1642	8150	7.2	1.13	1924	3.6	3.4
2	16	8	7670	7.4	1.04	1351	1701	4970	4.7	1.05	1886	4.4	3.6
2	17	9	9550	9.6	1.00	1355	1757	8430	8.2	1.03	1992	4.1	2.7
2	18	10	9560	9.1	1.05	1355	1768	27630	26.4	1.05	2242	4.2	1.7
2	19	11	14240	13.5	1.05	1310	1750	13970	12.4	1.13	2104	3.0	2.5
2	20	12	14530	13.7	1.06	1315	1866	8410	8.0	1.06	2066	3.7	2.3
2	21		14420	13.9	1.04								
2	22	13	10760	10.3	1.04	1350	1705	12210	11.0	1.11	2044	3.2	2.7
2	23		15610	15.4	1.01	1308	1938					3.9	
2	24	14	11620	11.5	1.01	1328	1826	11280	9.9	1.14	2078	4.2	2.2
2	25		19350	19.1	1.01								
2	26	15	16200	15.0	1.08	1302	1808	10300	9.0	1.14	2032	3.0	2.1
2	27		18040	17.8	1.01								
2	28	16	6690	6.4	1.04	1261	1503	15270	14.7	1.04	1967	3.5	3.0
2	29	17	9190	9.1	1.01			13180	12.4	1.07			
3.65	1	1	11790	11.3	1.04	1360	1798	13380	11.3	1.18	2052	3.6	1.8
3.65	2	2	12310	12.0	1.03	1274	1808	10680	10.1	1.05	2049	4.2	2.2
3.65	3	3	9940	9.8	1.01	1336	1897	12430	11.5	1.08	2092	5.5	1.5
3.65	4	4	13490	13.1	1.03	1341	1899	15310	14.8	1.03	2109	4.0	1.3
3.65	5	5	8720	8.5	1.02	1289	1730	11170	10.6	1.06	2020	4.9	2.5
3.65	6	6	10570	10.3	1.02	1299	1827	14860	14.2	1.04	2086	4.9	1.7
3.65	7	7	9350	9.2	1.01	1296	1791	15550	14.8	1.05	2080	5.1	1.8
3.65	8	8	10700	10.4	1.03	1335	1852	4910	4.8	1.03	2017	4.7	3.3
3.65	9	9	5480	5.3	1.03	1432	1726	8610	8.0	1.07	2021	5.2	3.3
3.66	1	1	9480	9.2	1.03	1307	1609	4610	4.2	1.09	1827	3.1	4.6
3.66	2		13190	12.7	1.04	1528	1854					2.4	
3.66	3	2	14590	14.3	1.02	1306	1816	20290	18.1	1.12	2101	3.4	1.4
3.66	4	3	15670	14.9	1.05	1303	1789	14230	11.6	1.23	2062	3.0	1.9
3.66	5	4	10790	10.5	1.03	1307	1777	9050	7.6	1.19	1962	4.2	2.0
3.66	6	5	13030	12.7	1.03	1364	1797	6490	5.6	1.17	1948	3.2	2.3

Table 1: Measurements of seismic geomorphological parameters for canyons and channel-levee systems.

3.66	7	6	11540	11.5	1.00	1347	1781	7510	7.0	1.08	1950	3.7	2.2
3.66	8	7	10020	9.9	1.01	1420	1949	14820	13.9	1.06	2157	5.1	1.4
3.66	9	8	11480	11.4	1.01	1299	2002	12840	12.5	1.02	2193	5.9	1.5
3.66	10	9	12150	11.8	1.03	1365	2075	27760	26.1	1.06	2434	5.7	1.3
3.66	11		11840	11.6	1.02	1383	2021					5.2	
3.66	12	10	11970	11.6	1.03	1381	2029	27990	26.4	1.06	2434	5.3	1.4
3.66	13	11	13020	12.1	1.08	1427	1985	29090	26.5	1.10	2434	4.2	1.5
3.66	14	12	7250	7.2	1.01	1455	1981	33200	28.6	1.16	2413	7.0	1.3
4	1		8700	8.2	1.06	1375	1951					6.4	
4	2		9250	9.1	1.02	1395	1980					6.1	
4	3	1	5010	4.5	1.10	1449	1887	15720	14.4	1.09	2126	8.5	1.5
4	4		6280	6.0	1.05	1683	1978					4.6	
4	5		6930	6.8	1.02	1572	1973					5.6	
4	6		6120	5.9	1.04	1558	1970					6.5	
4	7		6880	6.8	1.01	1529	1924					5.6	
4	8		10210	9.7	1.05	1569	2049					4.6	
4	9		5810	5.8	1.01	1565	1823					4.3	
4	10	2	7280	6.7	1.08	1580	1943	12030	10.1	1.19	2332	4.8	3.1
4	11		12700	12.2	1.04	1563	2132					4.4	
4	12		9100	8.6	1.06	1557	2078					5.6	
4	13		8070	7.5	1.08	1598	2094					6.0	
4	14	3	6000	5.7	1.05	1653	2030	37050	35.2	1.05	2894	6.1	2.3
4	15		5180	5.1	1.02	1574	2104					9.9	
4	16	4	5830	5.5	1.06	1607	2061	17430	15.4	1.13	2553	7.5	2.7
4	17		8200	7.8	1.05	1647	2234					7.0	
4	18		10370	10.1	1.03	1636	2321					6.4	
4	19		8190	7.9	1.04	1691	2271					6.9	
4	20		10420	9.9	1.05	1768	2376					5.7	
4	21		11290	11.1	1.02	1656	2400					6.4	
4	22		11190	11.0	1.01	1729	2460					6.3	
4	23		9040	8.8	1.03	1679	2434					8.1	
4	24		9760	9.5	1.02	1645	2345					7.0	
4	25		9040	8.4	1.08	1693	2435					7.9	
4	26	5	4770	4.7	1.02	1817	2277	29630	27.6	1.07	2894	9.3	2.0
4	27	6	3730	3.3	1.13	1805	2191	14040	10.8	1.30	2570	10.0	2.6
4	28		7640	7.4	1.03	1780	2326					6.9	
4	29	7	4350	4.2	1.04	1747	2252	28570	25.7	1.11	2894	11.2	2.2
4	30	8	5300	5.1	1.03	1753	2193	27620	25.0	1.10	2894	8.0	2.5
4	31		9580	9.2	1.04	1668	2383					7.2	
4	32		16040	15.3	1.05	1775	2516					4.5	
4	33		13750	13.5	1.02	1782	2526					5.3	
4	34		14320	14.4	1.00	1832	2526					4.7	
4	35		22650	22.1	1.02	1627	2797					5.0	
4	36		13580	13.5	1.01	1682	2701					7.3	
Average			**11551**	**11.2**	**1.03**	**1475**	**2010**	**15797**	**14.4**	**1.10**	**2190**	**5.0**	**2.3**
Minimum			**3726**	**3.3**	**1.00**	**1217**	**1503**	**4610**	**4.2**	**1.02**	**1827**	**2.4**	**1.2**
Maximum			**24739**	**22.2**	**1.14**	**1832**	**2797**	**45346**	**39.7**	**1.30**	**2894**	**11.2**	**4.6**

Table 1, cont.: Measurements of seismic geomorphological parameters for canyons and channel-levee systems.

Mass Transport Deposits

Zone	Perimeter (km)	Area (km2)	Length(km)	Width(km)	Angle(°)
4	85.1	507.6	27.5	21.62	1.5
1	102.1	366.1	38.4	13.66	0.7

Fans

Zone	Area (km2)	Length(km)	Width(km)	Angle(°)	Aspect Ratio
2	124.6	25.9	9.12	1.2	2.84
3	32.8	19.7	3.15	1.3	6.27
3	28.9	16.4	3.36	1.0	4.87
3	35.4	25.0	2.69	1.2	9.29
3	31.8	13.7	4.42	1.5	3.09
3	33.8	15.1	4.25	1.2	3.54
3	32.7	22.1	2.81	1.2	7.86
3	49.6	22.1	4.27	1.3	5.17
3	39.4	15.5	4.82	1.2	3.22
3	9.8	12.2	1.53	1.5	8.01
3	8.2	6.3	2.44	1.4	2.59
3	14.2	12.7	2.12	0.9	5.99
3	23.7	12.6	3.58	1.3	3.52
Average	**35.77**	**16.87**	**3.73**	**1.25**	**5.10**
Minimum	**8.16**	**6.34**	**1.53**	**0.86**	**2.59**
Maximum	**124.60**	**25.92**	**9.12**	**1.49**	**9.29**

Table 2: Measurements of seismic geomorphological parameters for MTD and fans.

RESULTS

REGIONAL SLOPE ARCHITECTURE

The seismic volume in this study area shows clinoforms with approximate 200 m topset to topset relief (Fig. 3B) developing on the shelf margin to slope. The clinoforms serve as an excellent reference to paleogeographic and sedimentary architectures of the basin, including the shelf break (transition on the up-dip section from flat to steep gradient), upper slope (steep upper section of the clinoform), lower slope (lower section of the clinoform), and toe-of-slope (flat section at the terminus of the clinoform) (Fig. 7).

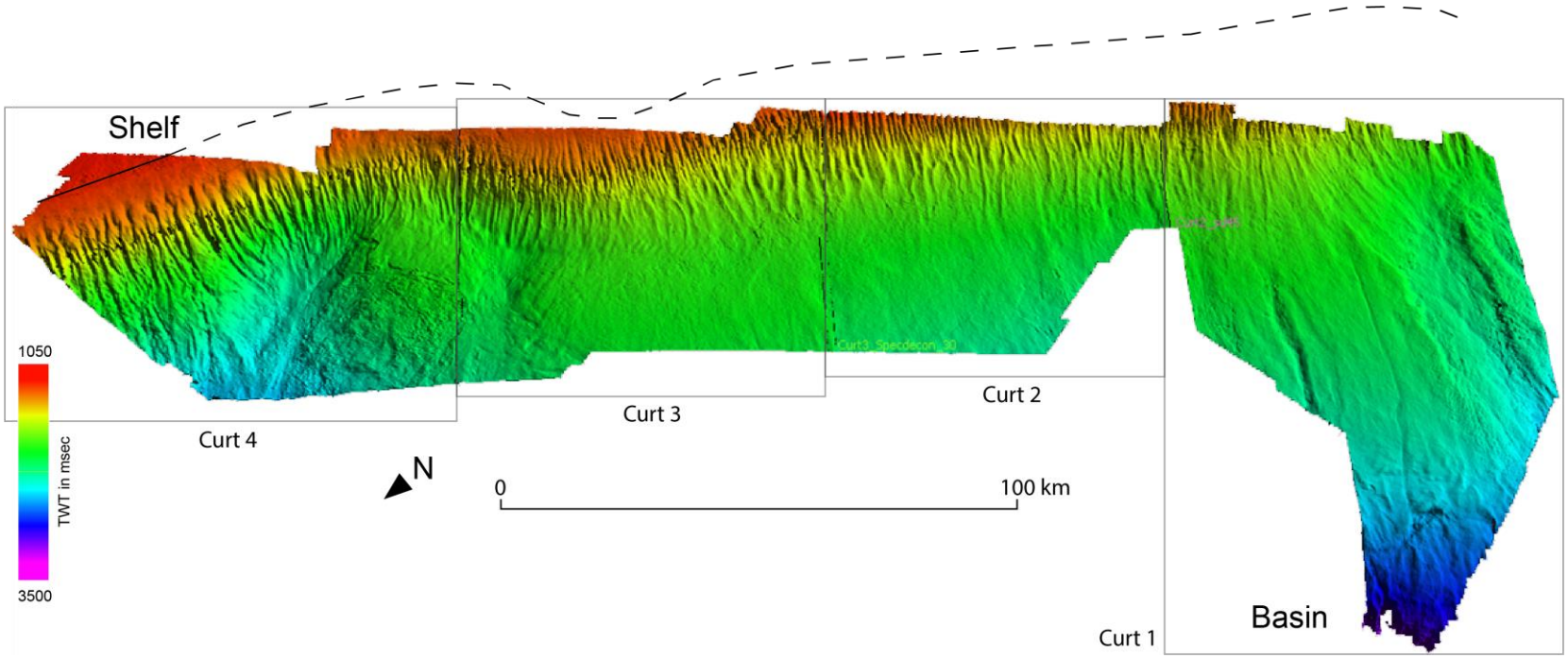

Figure 5: Time structure map of the study area. This map shows the paleogeography at the time of deposition. The shelf is situated to the east of the study area, and the basin is located to the west. Subregions Curt 1-4 are indicated by the gray boxes. The dashed line indicates the estimated location of the shelf edge. The region is separated into 4 subregions for later reference.

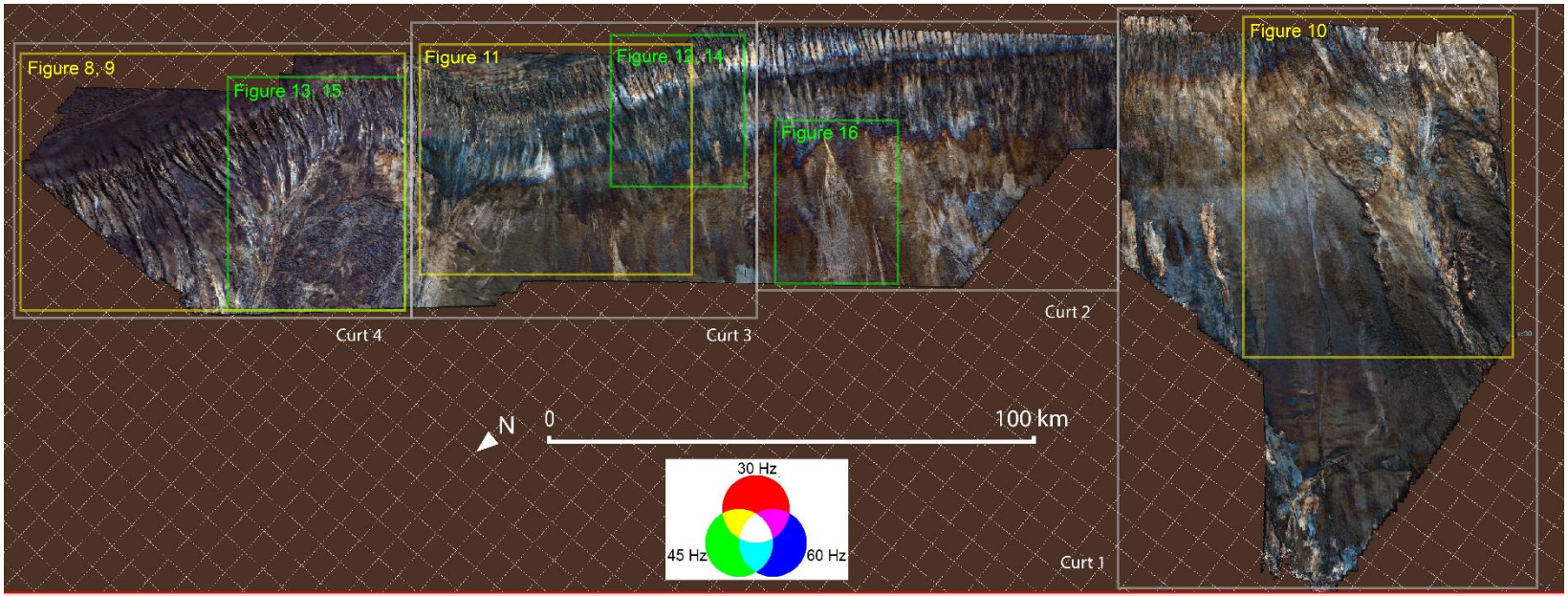

Figure 6: Spectral decomposition map of the study area. The spectral decomposition attribute is particularly useful for seeing the thickness changes of slope architecture. Yellow and green boxes indicate the location of close up views used in the figures of this paper.

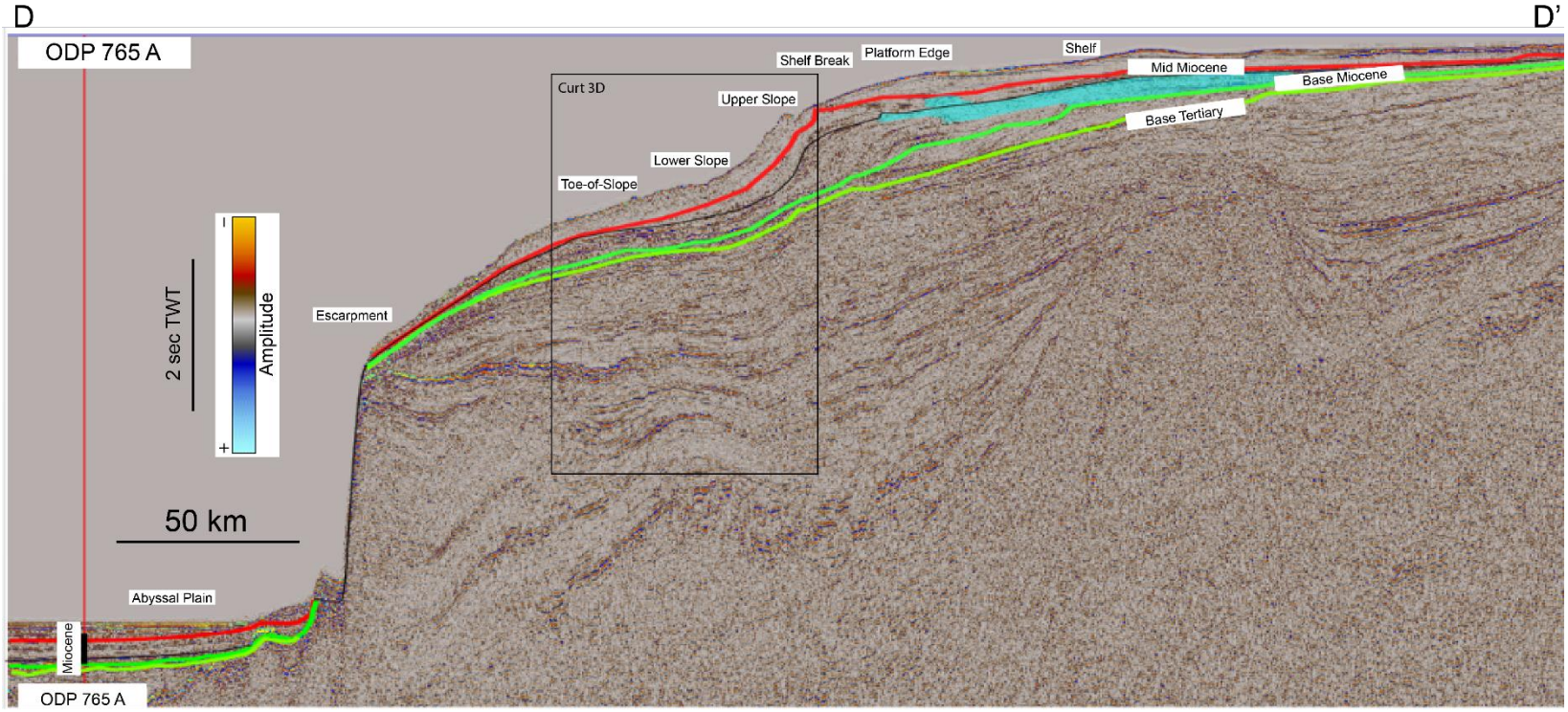

Figure 7: Regional cross section of the Browse Basin, outlining the structure from shelf to abyssal plain. The black box indicates the intersect with the study area.

At the regional scale, the study area is the central segment of a complete shelf-to-basin system (Fig. 4). The shelf consists of a more than 250 km wide and almost flat area. Differential compaction and later tectonic movement resulted in the shelf area dipping basinward into the present-configuration, but rotated flat-topped carbonate platforms shows that the shelf was almost flat at the time of deposition. The Miocene carbonate platforms developed within a 50-75 km wide zone at or near the continental shelf edge (Rosleff-Soerensen 2012, Belde et al. 2017, Tuyl et al. 2018). Carbonate platform growth cycle 3 (Fig 3B) prograded almost all the way to the shelf edge. Between carbonate platform margins and the continental shelf break, a 6-8 km wide area of low-angle non-channelized area called the outer shelf slope developed. The continental shelf break is the area where the depositional profile changes from a flat surface to a gradually seaward dipping surface with a 1.5° angle to a steep angle (up to 11°). It is the rollover of the regional clinoform that defines the older Oligocene and early Miocene shelf progradation. Past the shelf edge, the upper slope during the Miocene has a dip angle between 2.4 and 11°. Due to pre-Tertiary structural configurations, basinward of the steep upper slope, the slope angle decreases abruptly to an average of 2.3° for up to 100 km. This lower angle part of the slope, which we call the lower slope, continues until the structural escarpment approximately 150 km from the shelf edge. This fault-controlled-escarpment has a very steep slope (up to 90°) and drops abruptly more than 1500 m in bathymetry in less than 10 km. This has very similar geometry to other submarine escarpments like the Florida or Yucatan escarpments in the Gulf of Mexico (Bergantino 1971) or the western Atlantic edge of the Blake plateau (Sheridan et al. 1981). Beyond the escarpment is the modern-day Argo abyssal plain and its Tertiary equivalent (Fig. 1).

As seen in Fig. 3, morphology of the shelf during the Miocene is mostly flat, with local depressions likely related to structural inversion of pre-Tertiary rocks. Multiple cycles

of reef development reveal progradation, aggradation, and retrogradation of the platform (Belde et al. 2017), with the study interval (Phase 3) at the peak of platform expansion. In the study area, this platform can be seen in the northeast corner of the seismic volume (Fig. 8). Basinward of the study area, the depositional surface drops off into a second slope and finally into the abyssal plain (Fig. 7). In the study area, the shelf and slope morphologies during the Miocene can be expressed by the two-way time structure map at the base of the Miocene (Fig. 5). The shelf edge extends along the southwest to northeast (Fig. 5), with varying degrees of concavity. In this study, concavity will refer to the bend of the shelf edge in map view; positive concavity shelf edges bend towards the basin (Fig. 9 and 10) and negative concavity shelf edges bend landward (Fig. 11). Multiple canyons developed downstream to the northwest on a steep slope (> 10°). These canyons are spaced roughly 1-3 km apart. On the toe-of-slope, MTDs and other collapse features accumulated.

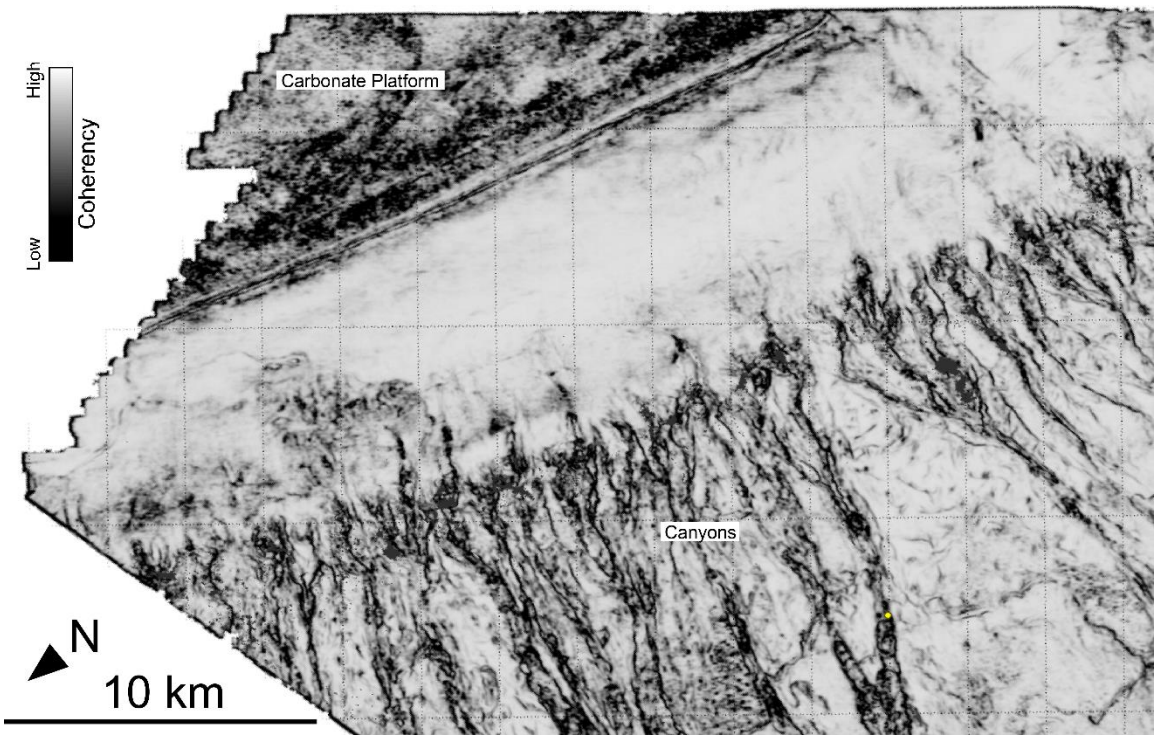

Figure 8: Shelf margin to slope transition, as seen on the north east corner of the study area in the coherency map view.

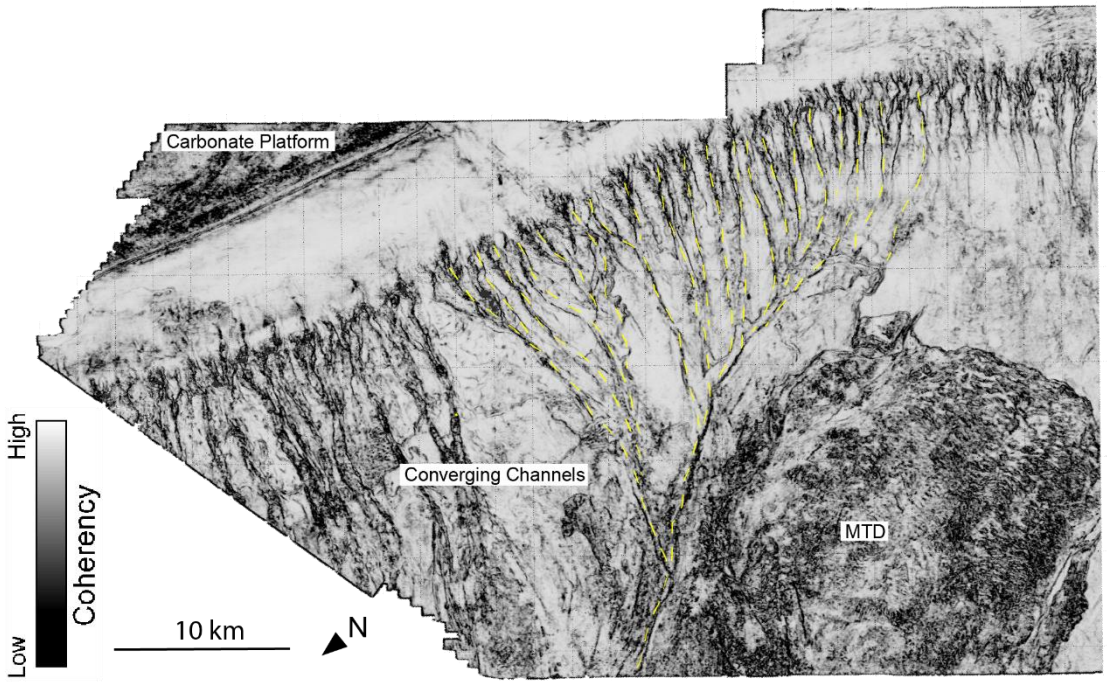

Figure 9: Convergent channels on a concave shelf edge, with channel rerouting by a MTD, as seen in the coherency map view.

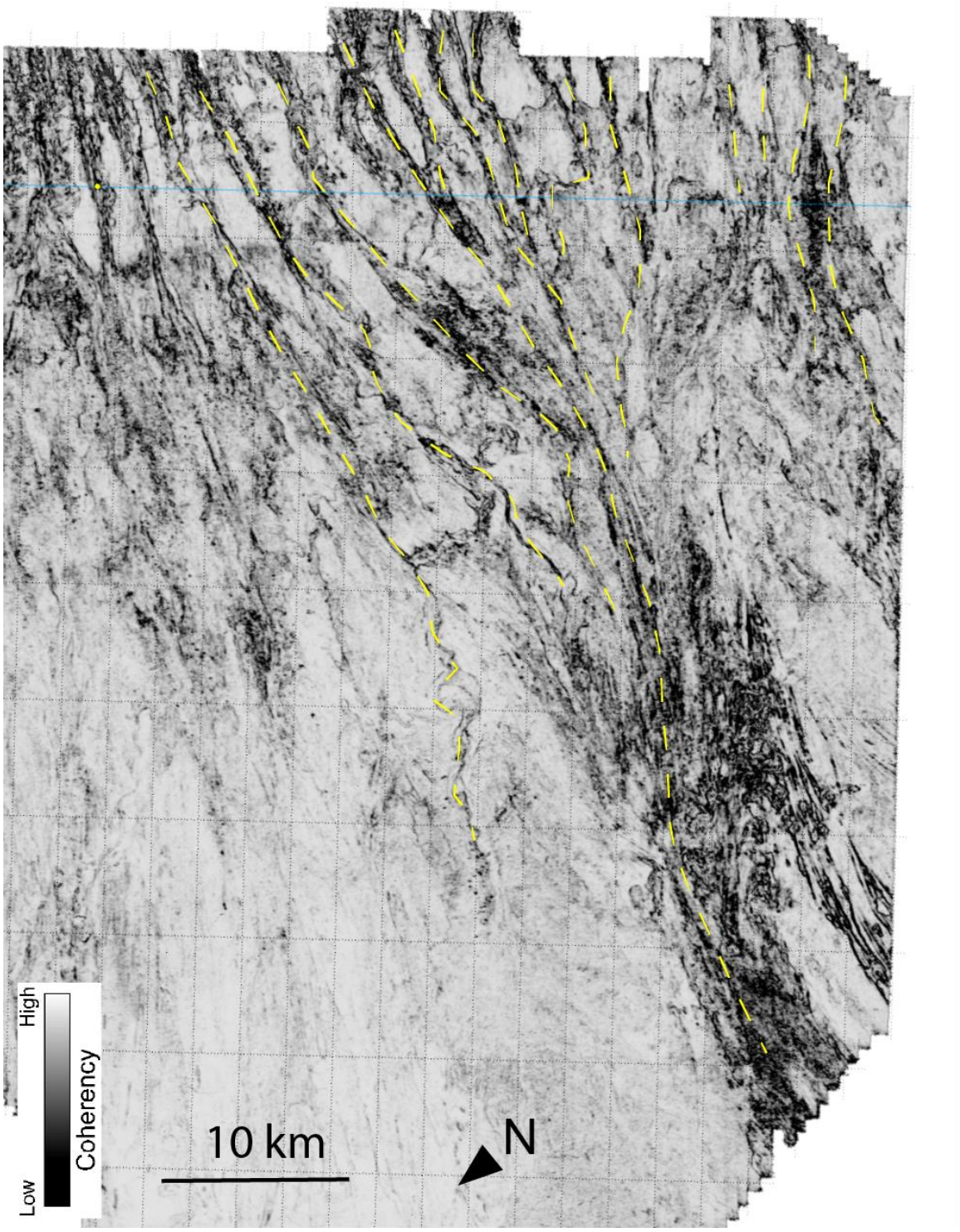

Figure 10: Convergent channels on a concave shelf edge, as seen in the coherency map view.

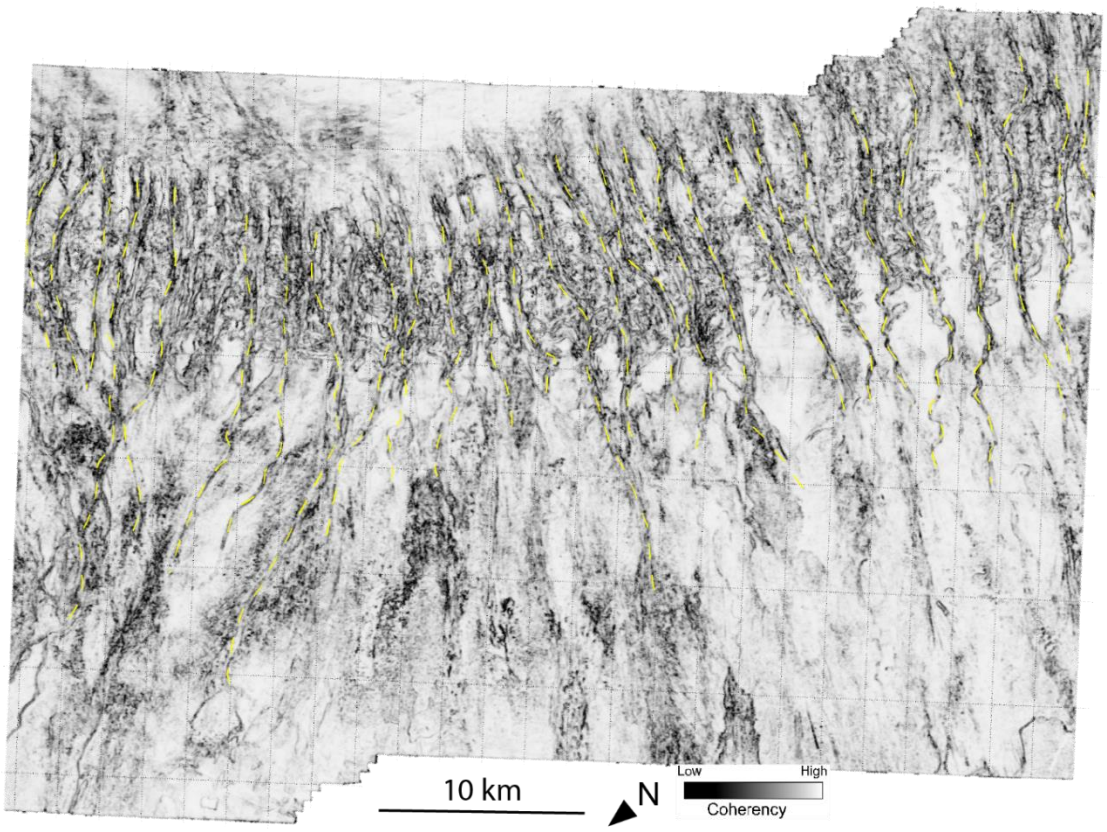

Figure 11: Divergent channels on a convex shelf edge, as seen in the coherency map view.

SEISMIC FACIES ANALYSIS

Seismic facies are ”mappable, three dimensional seismic units composed of groups of reflections that are different from adjacent groups of reflections (Mitchum et al. 1977). Analysis of seismic facies is used to identify recurring sedimentary archetypes with the purpose of describing and interpreting them. Several seismic facies were observed and quantified throughout the study area, based on methodology described by Mitchum et al. (1977). Seismic facies are defined using reflection amplitude, continuity, external

geometry, and internal architecture observed on the vertical sections, and spatial patterns and inter-relationships along horizontal coherency or spectral decomposition maps.

The first seismic facies represents thin (5-15 ms, or 18-25 m) and sinuous elongated channel-like forms, and is composed of several subfacies. In the cross-sectional view (Fig. 12A and 13A), high amplitude, medium frequency and continuous reflections (subfacies 1) on both flanks and a transparent to semi-continuous, u-shaped reflection (subfacies 2) along axis are observed. In a coherency map-view (Fig 12B and 13B) and spectral decomposition view (Fig. 12C and 13C), long and sinuous seismic lineaments are recognized (subfacies 3). Subfacies 1 and 2 form drapes with a flat bottom, convex top, and downlap on the underlying surface. These facies are found in the lower gradient areas near the end or past the large clinoforms. Most instances of this facies occur in the lower slope and toe-of-slope, where the angles range from 1.2 to 4.6°. The length of these facies in map-view range from 4.6 km to 45 km, with an average of 15.8 km. The geobody for this facies is also sinuous, with values ranging from 1.02 to 1.3 and an average of 1.10.

The second seismic facies recognized is of thick (50-150 ms or 80-250 m) elongated channel-like forms. This facies, similar to the first one, can be best observed through the coherency attribute on a map view as long, relatively straight features (subfacies). However, in the cross-section view, they appear to be larger and v-shaped (comparable to subfaces 2 in Fig. 12), and do not have the drapes protruding from the sides. Often, these geobodies are connected to instances of the first seismic facies. These facies are typically found embedded in the up-dip of the large clinoforms. Most instances of this facies occur in the upper slope to lower slope, with slope angles ranging from 2.4 to 11°. The length of these features in map view ranges from 3.7 km to 24 km, with an average of 11.6 km. The sinuosity for the body forms of this facies range from 1 to 1.14, with an average of 1.04.

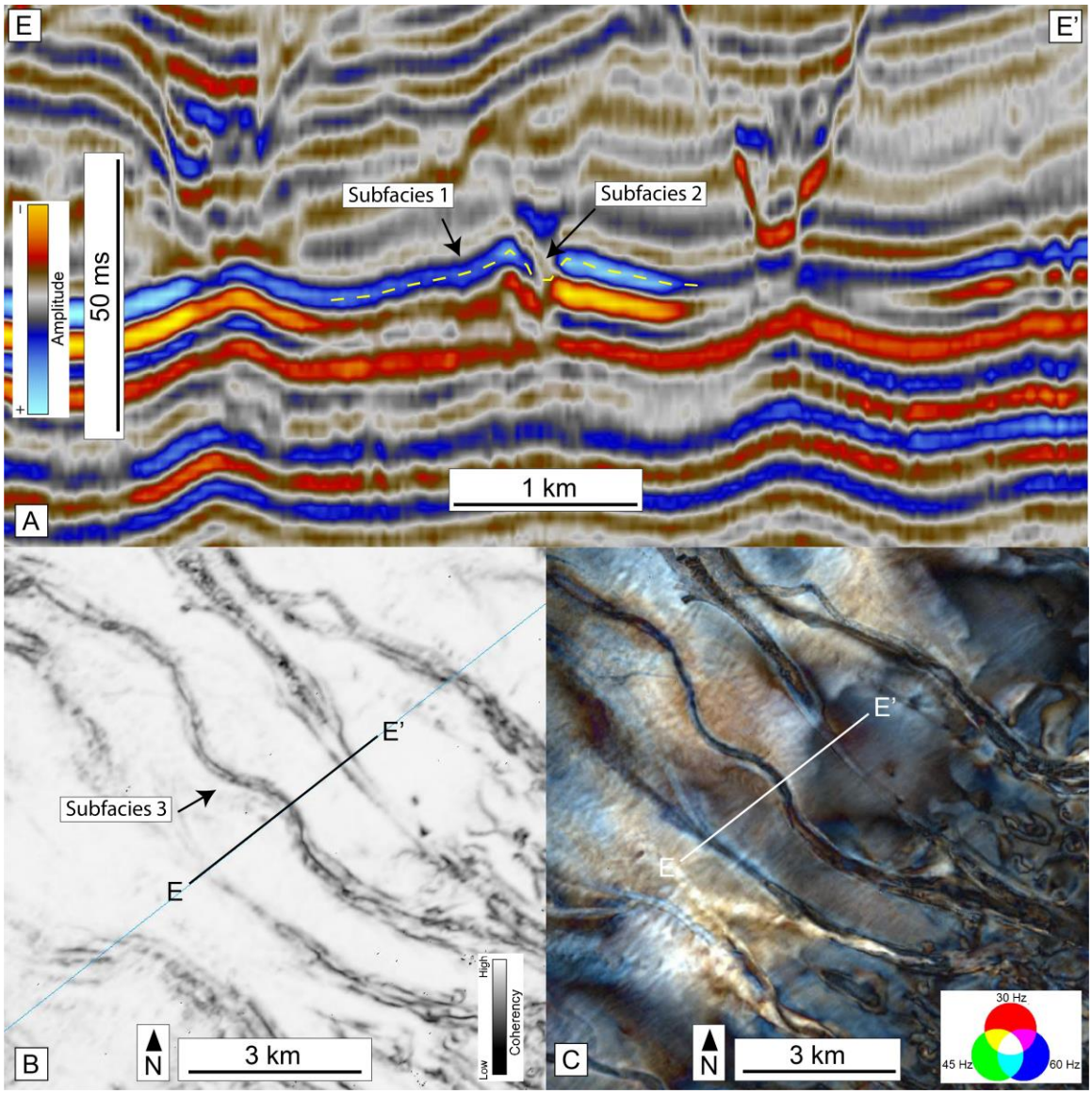

Figure 12: A) Cross section view of facies 1. Note the u-shape and the drapes disclosed by the seismic reflection marked in yellow. B) Coherency map view of facies 1. This facies can be identified by its sinuous and elongated form. C) Spectral decomposition map view of facies 1. Downdip direction is in the NW for both map views.

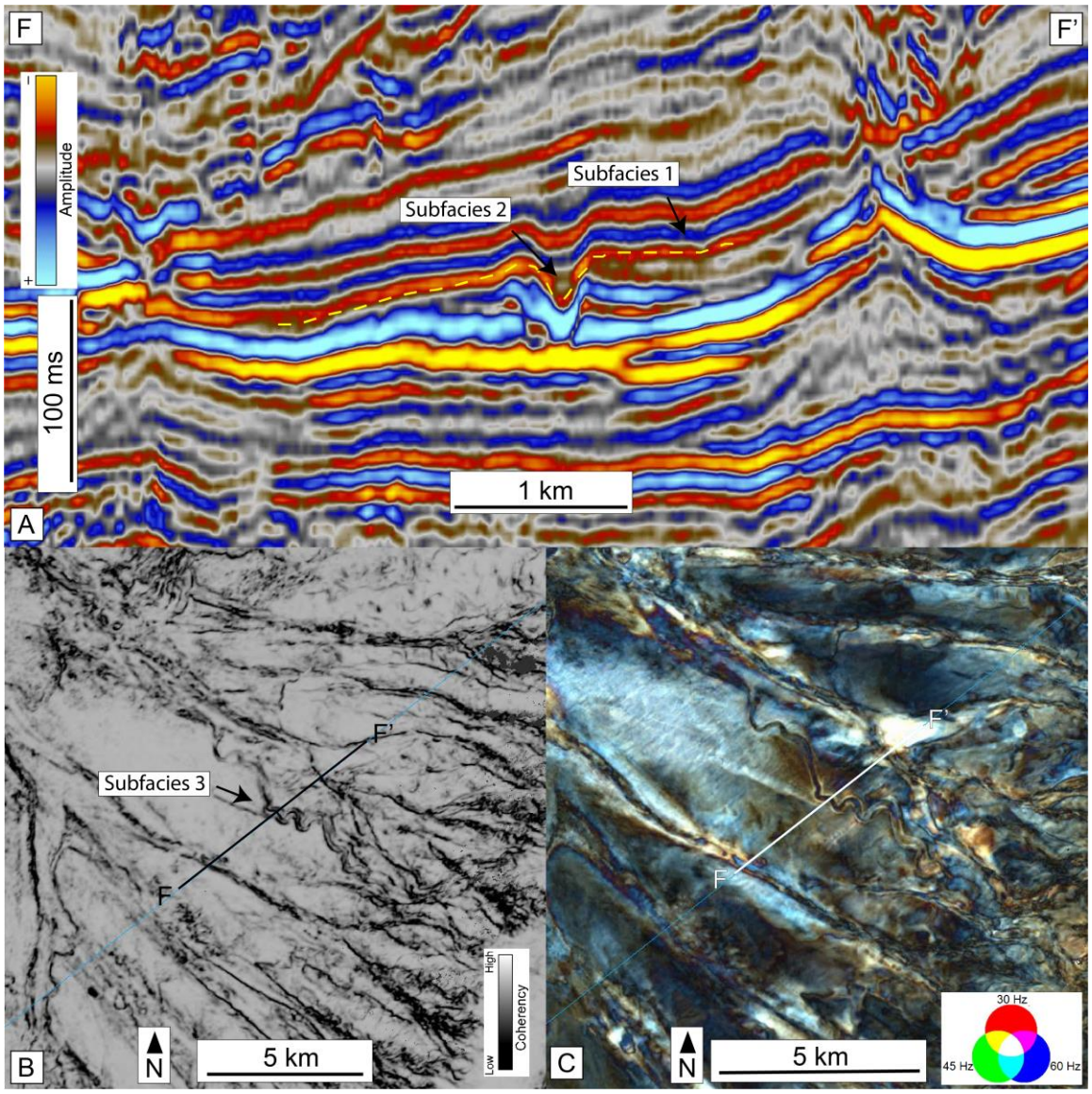

Figure 13: Another example of facies 1 in the study area. A) Cross section view, yellow dotted line denotes the outline of facies 1. B) Coherency map view of facies 1. C) Spectral decomposition map view of facies 1. Downdip direction is in the NW for both map views.

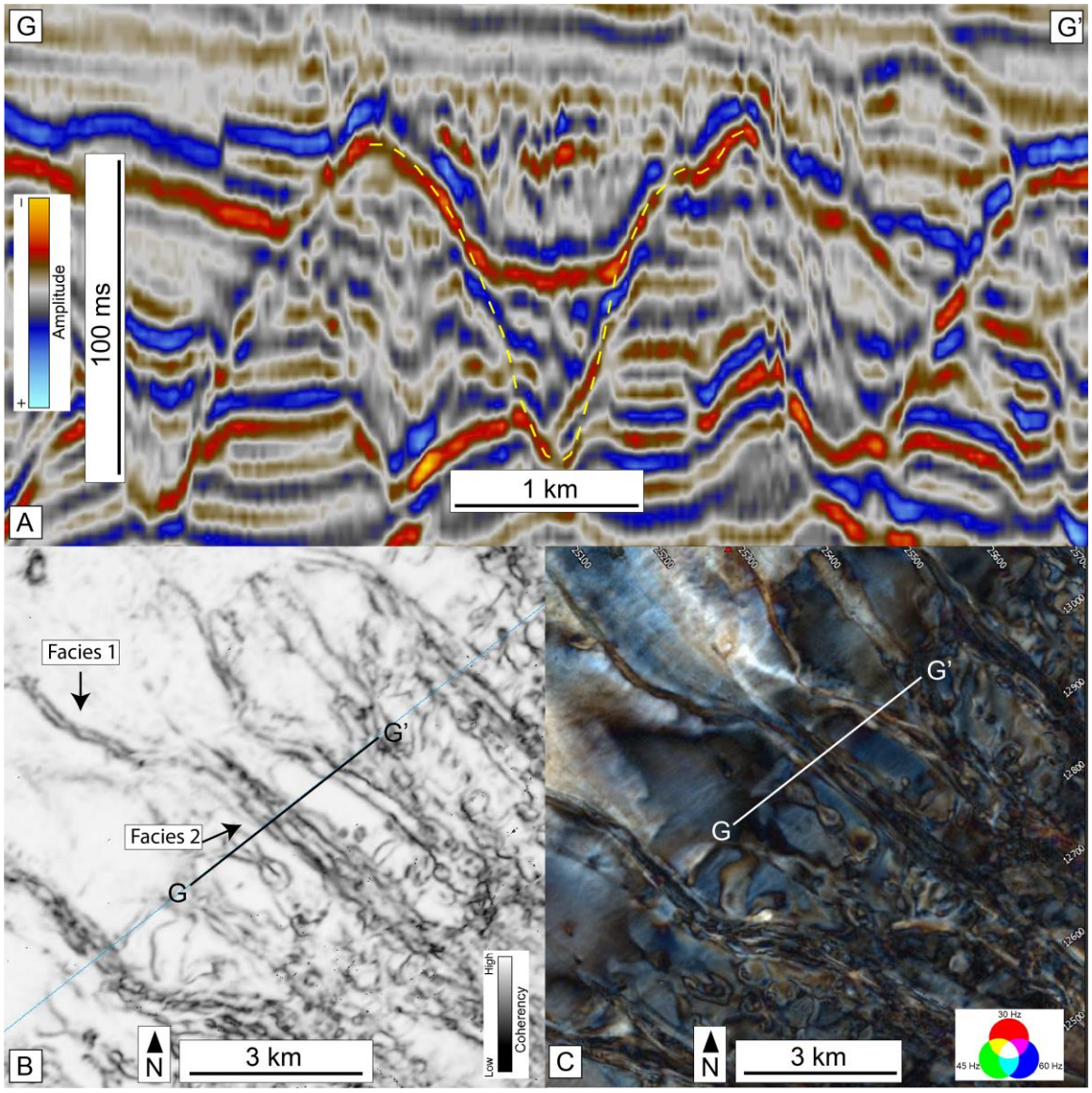

Figure 14: A) Cross section view of facies 2. Note the v-shape of the facies marked in yellow. B) Coherency map view of facies 2. This facies can be differentiated from facies one by its larger width and less sinuous nature. C) Spectral decomposition map view of facies 2. Downdip direction is in the NW for both map views.

The third seismic facies observed comprises large chaotic masses at the bases of the clinoforms, at the toe-of-slope. In coherency map view, they appear as large, elliptical masses. In the cross-section view, they appear as thick regions of chaotic reflectors that can span hundreds of kilometers along strike and dip. There are only two instances of this facies found in the study area, one spanning 507.6 km^2 and the other at 366.1 km^2. They are found at slope angles of 1.5 and 0.7°, respectively.

The fourth seismic facies observed comprises thin lens or sheet forms that are typically found attached to the end of facies one, although some are also found next to facies two. These facies are best viewed through the spectral decomposition attribute, which suggests that they are sensitive to thickness patterns. In the map view, they appear as large, triangular sheets. In cross section, this facies is barely perceptible, which may be due to how thin it is. Most instances of this facies are found within the Curt 2 and Curt 3 sub-volumes at the toe-of-slope region, with slope angles ranging from 0.9 to 1.5°, and an average of 2.5°. The size of these facies ranges from 8 to 120 km^2. The elongation can be measured using aspect ratio (length/width), which ranges from 6 to 26.

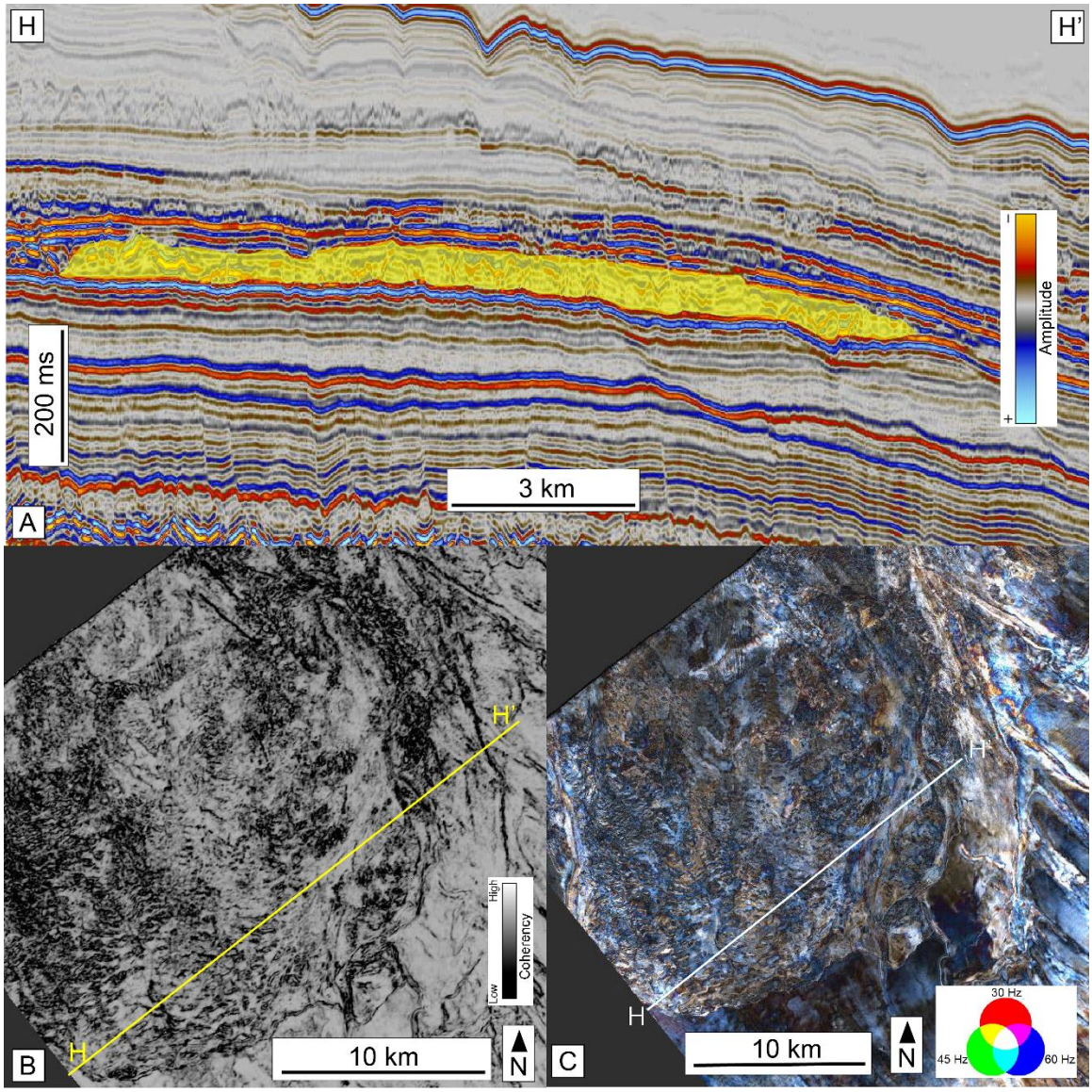

Figure 15: A) Cross section view of facies 3. Interpreted facies is highlighted in the yellow shaded area. B) Coherency map view of facies 3. C) Spectral decomposition map view of facies 3. Downdip direction is in the NW for both map views.

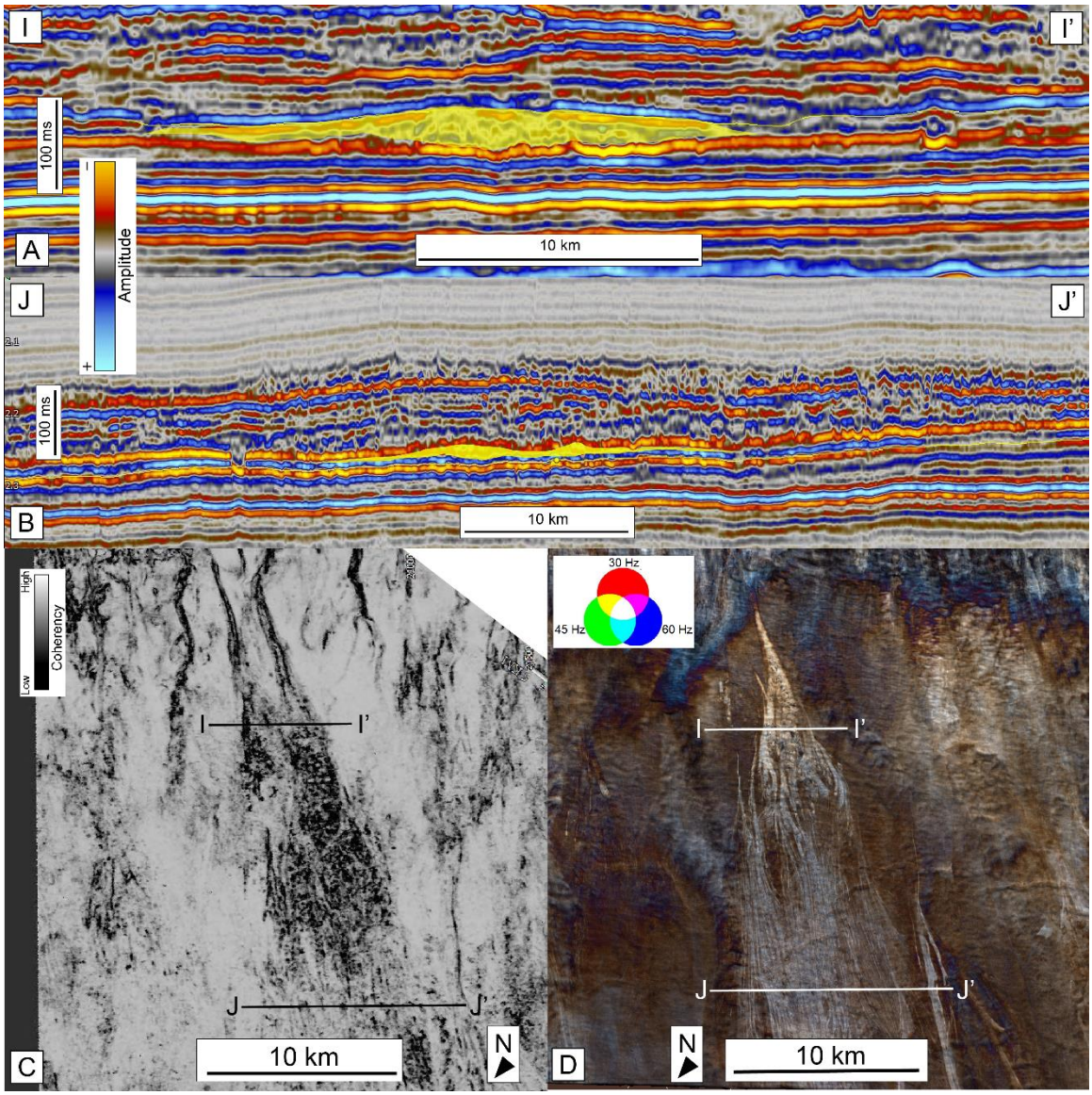

Figure 16: A) Cross section of facies 4 at the more proximal end of the lower slope. Compared to the (B) distal cross section, the facies 4 unit is thicker, but less spread out. C) Coherency map view of facies 4. Note the triangular shape of the facies. D) Spectral decomposition map view of facies 4. Downdip direction is in the NW for both map views.

INTERPRETATIONS

SLOPE ARCHITECTURAL ELEMENTS

Normark et al. (1987) defined architectural elements as erosional or depositional features that can be mapped in ancient or modern systems. In this study, architectural elements will refer to depositional features found on slopes – canyons, channel-levee systems, MTDs, and fans. Canyons are generally deep, wide, and v-shaped incisional channels found on steeper slope angles (Normark et al. 1993). Channel-levee systems are channels that are shallower, narrower, and more sinuous than canyons, and are found on gentler slope angles. They also feature levees, which are aggrading sediment overbanks on either side of the channel (Posamentier and Kolla 2003). MTDs are large depositional features formed from slides, slumps, or gravity flows, and fans are smaller depositional features that are essentially unconfined frontal splays at the end of channels (Posamentier and Kolla 2003). The four seismic facies noted in the observation section above were interpreted to be various architectural elements found in a slope system.

The first facies is interpreted to be channel-levee systems (Fig. 17, blue lines), judging by the u-shape center and long wing-like wedges spreading from both sides (Posamentier and Kolla 2003). These channels are sinuous (1.02-1.3), and occupy the lower slope (average slope angle of 2.5°). The wedges that flank the channel forms in the cross section are interpreted to be levees.

The second facies is interpreted to be submarine canyons (Fig. 17, red lines). These canyons are less sinuous (1 – 1.14), and occupy the upper, steeper slopes (average slope angle of 5.0°). The V-shape of their cross sections suggest that the canyons formed by cutting into the slope, although at the lower slope, the cutting behavior transitions to a depositional behavior (Posamentier and Kolla 2003). The relatively evenly spaced

distribution of the canyons along the slope aligns with the line-fed depositional pattern often found on carbonate slopes.

For the third seismic facies, the chaotic reflection attributes and their large size (500 and 360 km^2 in area) suggest that they are best interpreted as MTDs (Posamentier and Martinsen 2010). These features are found in the lower slope, with slope angles of 1.5° and 0.7° (Fig. 17, green lines). The MTDs in the study area were likely formed before the development of nearby channel-levee systems, causing them to detour around the edge of MTDs (e.g., the channel-levee systems and MTD in Curt 4, Fig. 16).

The fourth facies is located at the terminus of various channel-levee systems and canyons at the lower slope (average slope angle of 1.3°). This fourth facies has a lobate plan view and its subparallel layered internal reflections in its cross section gradually thins away from the central axis. The thinning nature of this facies and its location relative to the slope would suggest that it is some kind of unconfined splay or fan (Posamentier and Kolla 2003). They are marked in Fig. 17 as orange arrows.

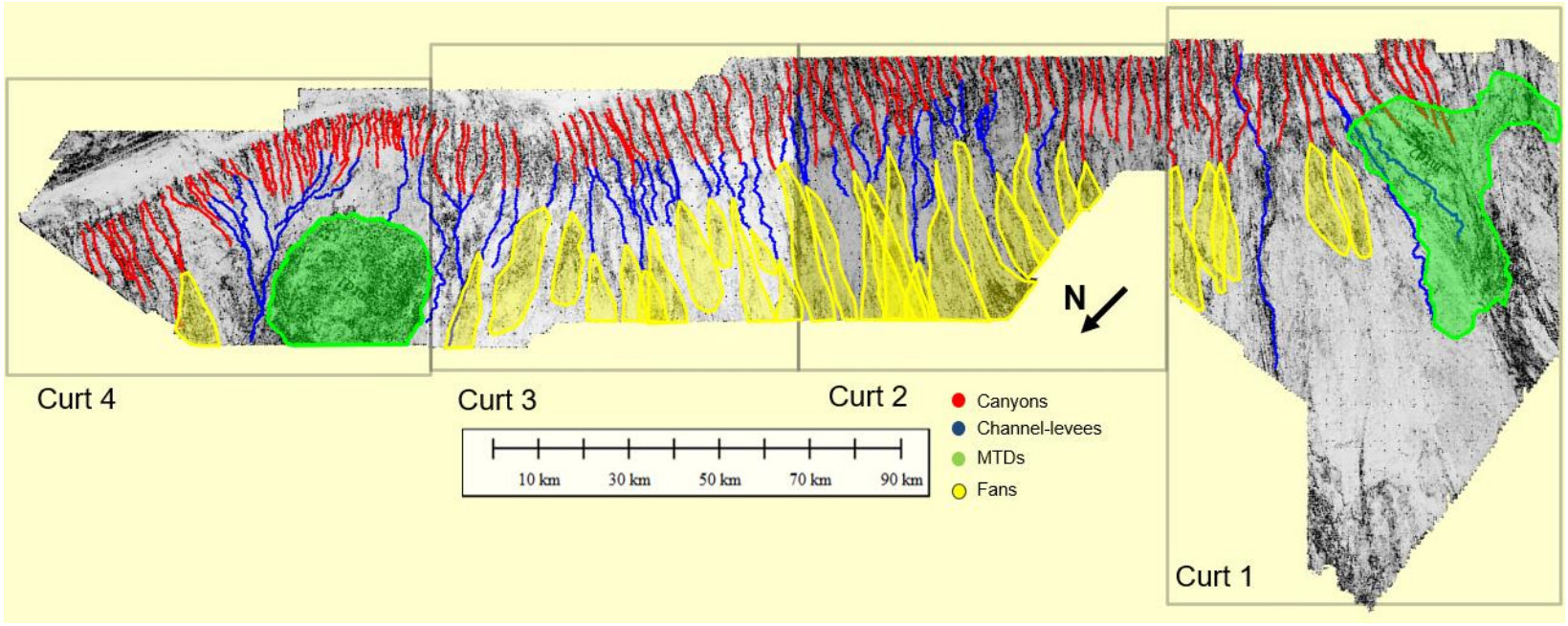

Figure 17: Coherency map showing the interpretation of seismic facies. The distribution of facies is regulated by the gradient or position on the slope.

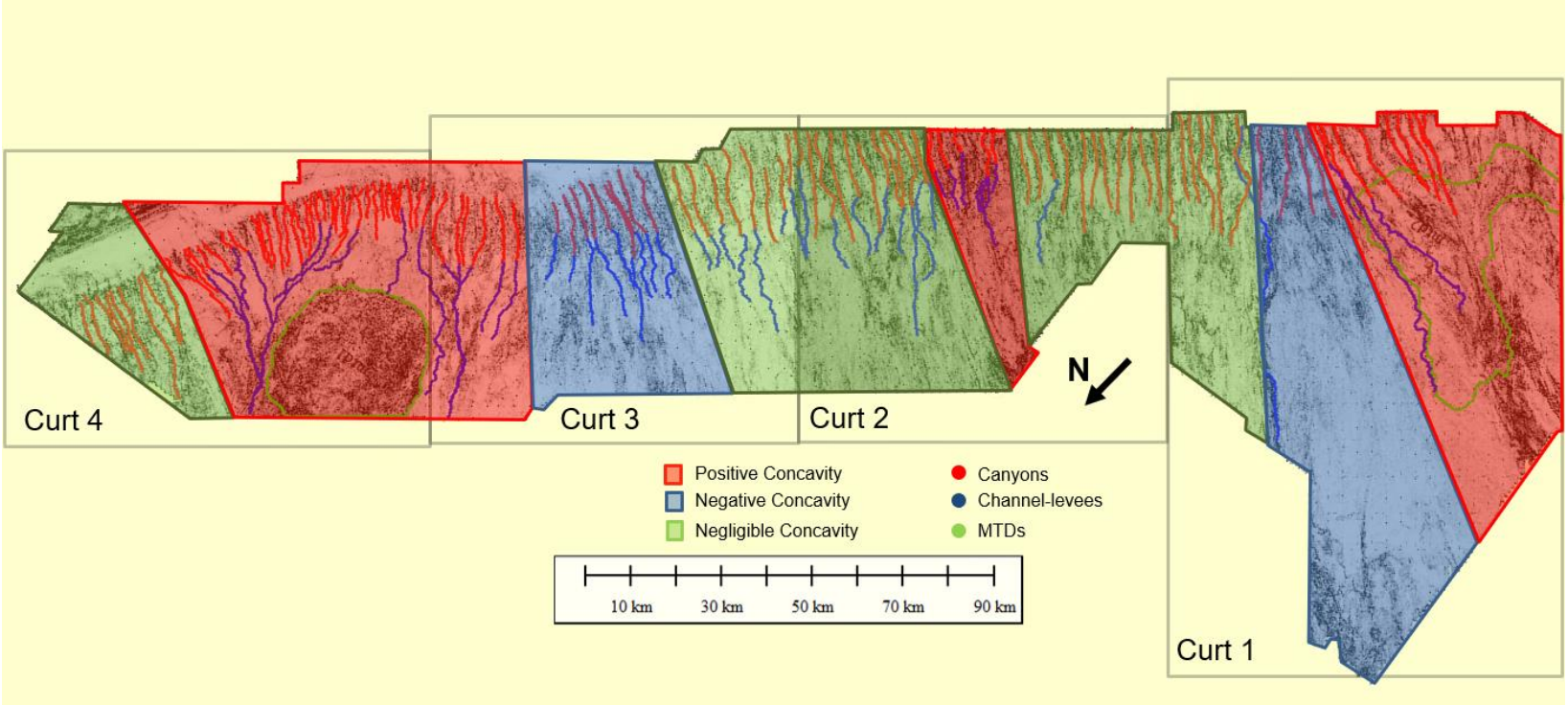

Figure 18: Shelf edge concavity controls the convergence or divergence of channels downslope.

SHELF-SLOPE MORPHOLOGY CONTROLS ON ARCHITECTURAL ELEMENTS

The shape of the shelf edge can influence the behavior of channels (Fig. 3). Concavity of the platform edge seems to play a prominent role in determining channel convergence. In the southern side of Curt 4, the inward concavity of the shelf edge, as well as the placement of the MTD, forces the channels to congregate around the MTD and form large channel-levee systems. These combined channels tend to express high sinuosity, and likely extend past the second slope into the abyssal plain (Fig 4). Conversely, in areas where the shelf edge convex outwards, channels tend to diverge, are shorter in length, and the basin sediment deposits are somewhat common. This can be seen in the Curt 3 sub-volume in Fig. 17. In Fig. 18, the study area was divided according to shelf edge concavity. Canyon and channel-levee system statistics divided by concavity zone can be found in table 3 below.

In areas with positive concavity, canyons ranged from 3.7 to 19 km in length, 1-1.13 in sinuosity, and slope angle of 5.0 to 21.6o with an average of 11.7, and the channel-levee systems had ranged from 5 to 45 km in length, 1.05 to 1.3 in sinuosity, and slope angle of 1.2 to 4.0°, with an average of 2.4^{o} (Table 3).

The study area had relatively small areas with negative shelf edge concavity compared to positive or straight concavity, but the data collected can still be compared to that of areas with positive concavity. Channel-levee systems found here are much shorter (average of 11.4 km compared to 20 km in positive concavity areas) and less sinuous (average of 1.05 compared to 1.11 in positive concavity areas). Canyons were slightly longer in negative concavity areas (average of 13.5 km compared to 0.9 km in positive concavity areas). All other factors, such as canyon sinuosity and slope angles for both canyons and channel-levee systems, are mostly the same.

Channels in regions with straight shelves mostly exhibit statistics that are in between that of the two regions previously discussed, but are closer to that of the negative concavity region. The only exception is the channel-levee system sinuosity (average of 1.10), which is close to that of positive shelf concavity regions, and canyon slope angle (average of 4.1°), which is lower than both other regions.

These data show a similar trend to that of siliciclastic submarine slope channels (Posamentier 2003) and other carbonate submarine slope channels (Janson pers. comm. 2018), with straight canyons occurring in the steeper slope and more sinuous channels in the lower angle slopes.

Positive Concavity Channels (54)						
	Canyon Length (m)	CLS Length (m)	Canyon Sinuosity	CLS Sinuosity	Canyon Angle	CLS Angle
Average	9260	20050	1.04	1.11	6.0	2.4
Minimum	3730	4970	1.01	1.05	2.5	1.2
Maximum	19310	45350	1.14	1.30	11.2	4.0
Negative Concavity Channels (10)						
	Canyon Length (m)	CLS Length (m)	Canyon Sinuosity	CLS Sinuosity	Canyon Angle	CLS Angle
Average	13510	11350	1.03	1.05	5.8	2.5
Minimum	5480	4910	1.00	1.02	2.5	1.2
Maximum	24740	15550	1.11	1.07	11.2	4.0
Straight / Neglegible Concavity Channels (45)						
	Canyon Length (m)	CLS Length (m)	Canyon Sinuosity	CLS Sinuosity	Canyon Angle	CLS Angle
Average	13770	12560	1.03	1.10	4.1	2.3
Minimum	6690	4610	1.00	1.03	2.4	1.2
Maximum	22650	27630	1.08	1.23	11.2	4.6

Table 3: Statistics for canyons and channel-levee systems (CLS) for each shelf edge concavity

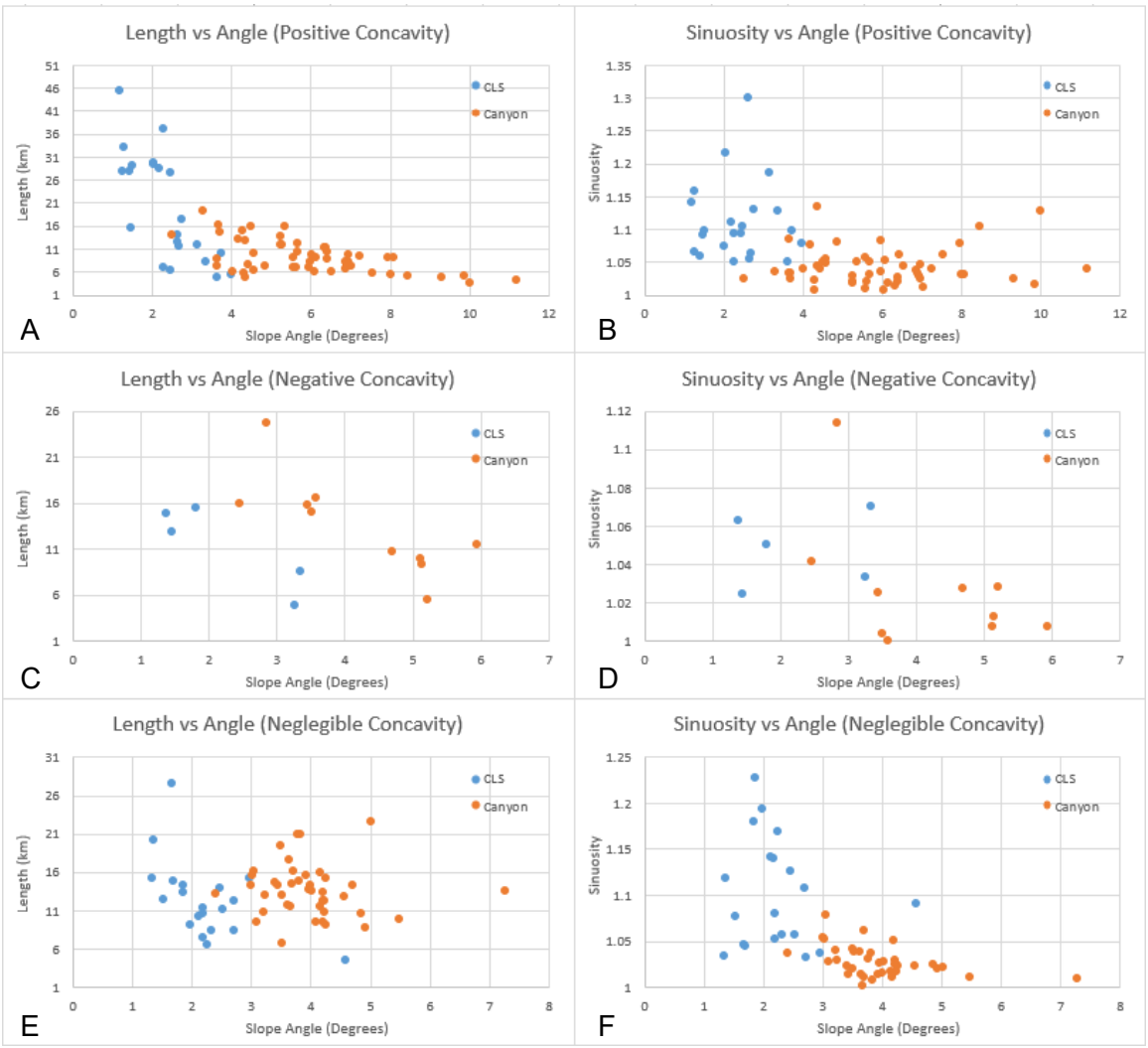

Figure 19: Cross plots comparing length, slope angle, sinuosity and concavity for canyons and channels. For positive concavity, canyons are characterized by larger slope angle, shorter length (A) and lower sinuosity (B) than channel-levee systems. For negative concavity, canyons are characterized by larger slope angle but similar length (C) and sinuosity (D) to channel-levee systems. Where concavity is negligible, canyons reveal a larger slope angle but a similar length to channel-levee systems (E), and a lower sinuosity (B) than channel-levee systems (F).

In all cases, higher sinuosity is measured when the slope angle is lower. Channel-levee systems in positive concavity shelf edges seem to adopt a negative correlation between channel length and slop angle. They also exhibit significantly more length than other shelf concavities, and are slightly more sinuous (Fig. 19).

Additionally, twelve fans were interpreted within the study area. Marking the terminus of channel-levee systems, they are mostly found in the Curt 2 and Curt 3 sub-regions, where they can be best seen through the spectral decomposition attribute (Fig. 16D). It is possible that the ends of the channel-levee systems in the Curt 1 and Curt 4 sub-regions also have fans; however, because these channels often extend past the study area, it had not been observed.

A depositional model is proposed (Fig. 20) that attempts to explain the effects of shelf edge concavity, slope angle, and topographical obstructions. In a carbonate slope environment, slope angle determines canyon/channel sinuosity, with canyons in the steeper upper slope less sinuous than the channels occurring in the gentler lower slope. Combined effects of shelf-edge concavity and MTDs developed in the toe-of-slope makes the channels reroute around obstacles under gravity, forming characteristic facies patterns in positive concavity and negative or negligible concavity zones.

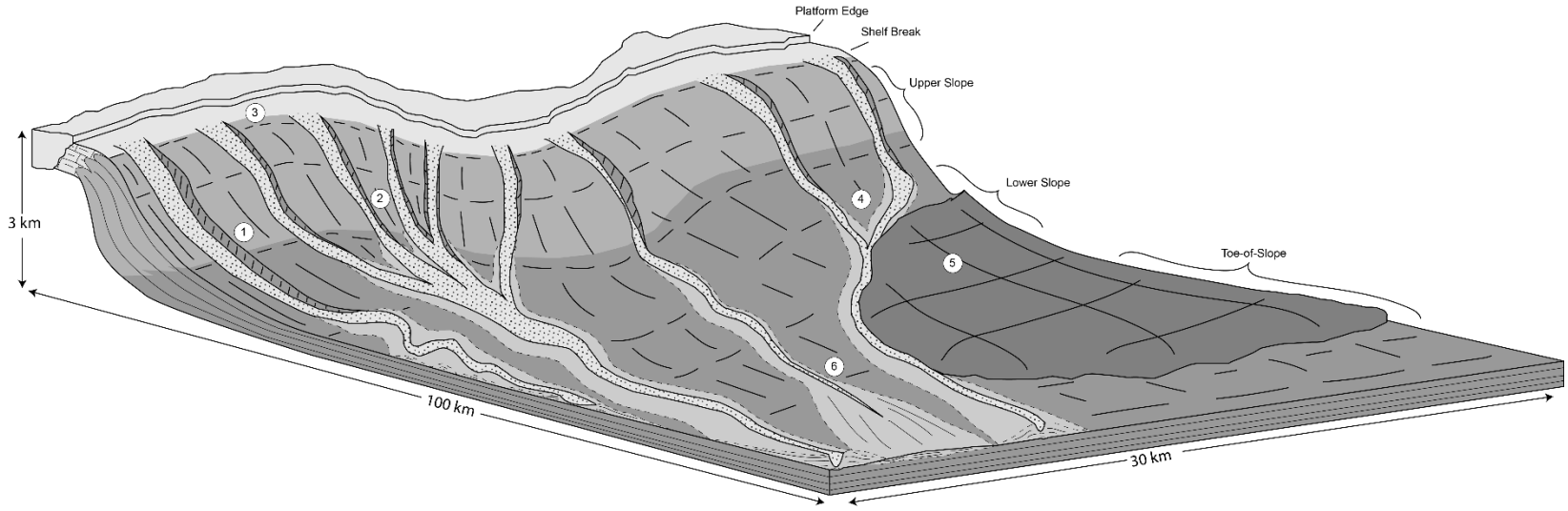

Figure 20: Idealized model of a carbonate slope influenced by shelf edge concavity. 1) canyon and channel-levee system with negligible concavity. 2) channel convergence with positive shelf edge concavity. 3) continuous reef along the shelf edge. 4) effect that obstacles, such as MTDs (5), have on rerouting channels on the lower slope. 6) fan lobate system deposited in the lower slope. The shading indicates the region of the slope, with (7) indicating shelf edge to upper slope transition, (8) indicating upper slope, and (9) indicating lower slope and toe-of-slope.

DISCUSSION

REGIONAL CONTROL

The tectonic history has played a critical role in shaping the carbonate system in the study area. The structure of the Browse Basin developed during Jurassic rifting, when a series of half-grabens were established that strike parallel to the shelf margin (Veevers and Cotterill 1978, Struckmeyer et al. 1998). A series of progradational carbonate sequences was deposited during the Eocene to Oligocene, forming a carbonate ramp shelf-slope system (Apthorpe 1988, Rosleff-Soerensen et al. 2012), which would make up the antecedent topography on which the Miocene clinoforms developed (Fig. 2). Reactivation of the Jurassic faults caused by an oblique collision between the Pacific and Australasian plates during the late Oligocene to early Miocene (Rosleff-Soerensen et al. 2012) generated some tectonic inversion in the Browse Basin (Keep et al. 2000), but does not seen to have any significant effect on the study area. No evidence of tectonic movement or syntectonic sedimentation during the middle Miocene can be seen in the seismic survey.

Sediment influx in the study area was likely supplied by a series of carbonate banks of Miocene age (Belde et al. 2017, Fig. 3A). The study interval correlates to the third cycle of carbonate growth. This cycle is marked by an extensive platform rimmed by a continuous barrier reef along the shelf margin and patch reefs in the shelf interior (Belde et al. 2017), and is responsible for significant progradation of the margin in the study area (Fig. 3B, Janson pers. comm. 2018) as it kept up with higher subsidence and accommodation rates (Belde et al. 2017). Compared to the 3rd carbonate growth interval of Belde et al., the underlying second cycle also featured significant progradation of the margin (Fig. 3B), but did not extend far enough into the study area to have a comprehensive overview. Regionally, this second growth phase is almost always narrower than the third

growth. The overlying cycle 4 corresponds to the initiation of regional drowning of the shelf. Carbonate platforms in cycle 4 are much smaller in size and completely drowned almost everywhere. Similarly, the slope associated with cycle 4 retreated, and the volume of sediment on the slope is an order of magnitude less than the previous slope interval. There is therefore a correlation between cycle 3 being one of the largest carbonate platforms with its complex slope architecture, including numerous aggrading overbank wedges between submarine canyon and levees developing with the sinuous channels. The increase of a shallow water carbonate platform likely increased the amount of sediment produced on the platform top, which could potentially increase the amount of reworked sediment from the carbonate platform to the slope. The horizons used for this study were taken from the sediments at the peak progradation. The slope systems, including canyon, channel and levee systems, fans, and MTDs, all expressed complete patterns and maximum extension.

Angles of carbonate slopes have been well documented in previous studies (Playton et al. 2010, Janson et al. 2011, Adams and Schlager 2000, Kenter 1990). Most carbonate slopes have a wide range of slope angles of starting from around 30° at its steepest, with some reef-rimmed escarpments reaching a completely vertical slope, and reaching much lower slope angles at the lower slope. The slope angles recorded in this study only reach up to 11° slope angle at the steepest, which would place the carbonate slope of this study area on the less steep side of carbonate slopes around the world.

Playton et al. (2010) also differentiated between two types of margins. The first type is the escarpment margin, where the shelf is decoupled with the slope, and slope mostly onlaps with the escarpments. The second type of margin is the accretionary margin, where the margin transitions relatively smoothly into accretionary clinoforms, and where the margin can aggrade, retrograde, or prograde depending on sediment influx, sea level,

or subsidence. The slope in this study falls in the category of accretionary margins, due to the lack of escarpment and the presence of clinoforms. Furthermore, Playton et al. (2010) also describe several kinds of accretionary margins. The slope of this study would fall under the prograding margin with sigmoidal clinoforms, as described in the modern leeward Great Bahamas Bank. This subcategory emphasizes a prograding shelf margin and vertical accretion of the entire slope region due to increases in shelf sediment production, high shelf-to-slope sediment transfer, and separation between the carbonate platform and slope (described below), which are similar to the system described here.

Hurd et al. (2016) describes a unique type of carbonate slope where there is a considerably wide (4-6 km) outer shelf separating the escarpment of the carbonate platform and large-scale inflection point (LSI), the point where the slope transitions from a flat outer shelf to the upper slope. This also describes the shelf to basin system in the study area, where there is a 6-8 km low-angle (approximately 1.2°) outer shelf separating the LSI and the small (200 m relief) and short (500 m wide) steep slope of the carbonate platform. This is different than classical shelf-to-basin carbonate models described elsewhere (Playton et al. 2010), where the slope is attached directly to the carbonate platform. However, what makes this particular outer shelf region different than the ones described in Hurd et al. (2016) is that it is not channelized. Sediment seems to bypass this area from the carbonate platforms to the slope without eroding anything. A similar phenomenon can be seen in the Little Bahamas Bank (Mulder et al. 2017). Past the LSI is where the sediment flow becomes confined and erosive.

The shape of a slope is a function of its antecedent topography, sediment supply, and depositional environment. Adams and Schlager (2000) identified three different slope forms – the planar curvature, which can be described by a straight line, the concave-up curvature, in which the slope is only concave in, and the sigmoidal curvature, in which the

upper slope is convex out and lower slope is concave in, similar to a Gaussian distribution. The slope profile of this study correlates to the sigmoidal morphology slope described above. Schlager and Adams (2001) suggest that these kinds of slopes take their shape from the decay of sediment transport due to the increasing distance to the basin over time, and remodeling of the shelf break from sea-level fluctuations or storms.

COMPARISON TO SILICICLASTIC SLOPES

Playton et al. (2010) summarize many differences between carbonate and siliciclastic slopes, from grain sizes to depositional patterns. In particular, carbonate slopes feature early lithification, high slope gradients, coarse debris, and line-fed sediment dispersal (requires sediment focusing mechanisms for downslope point source), while siliciclastic slopes in comparison generally have lower lithification and common sediment redistribution, lower gradients, less coarse debris, and point-sourced sediment dispersal. These characteristics do not define all unique carbonate or siliciclastic slope systems, but do apply to them in general.

In siliciclastic slopes, material influx is largely formed from detrital sediment originating from terrestrial channels, deltas, and longshore drifts. As such, channels that appear on the submarine slope are largely point-sourced, and can extend well into the down the slope and into the basin (Gee et al. 2007, Piper and Normark 2001).

In contrast, the classical carbonate slopes exhibit none of those features. As sediment accumulates on the shelf, it is eventually pushed out into the slope as line-fed aprons, where the traditional view is that they collapse into turbidites or gravity flows (Mullins and Cook 1986, Playton et al. 2010). Previous modern slope studies and our results however indicate that this slope apron model needs to be revised. With higher resolution data provided by modern multibeam data or 3D seismic data, the classic apron

seems to be in fact a more or less coalescence of many line-sourced systems. Each line source system can potentially have its own either complete or partial set of architectural elements, such as canyons, sinuous channel-levee systems, and fans, all with various lengths and architecture. At the larger scale, each of these line source systems overlap and superimpose with each other, depending on the slope morphology and evolution. In addition, other deeper processes, such as slope collapses, can modify and interact with these complex sets of line source systems. The resulting overall architecture remains a large apron of carbonate sediment being deposited on the slope, but its internal architecture is much more complex than previously thought. As a result, the point-source vs line-source differentiation is really a question of scale and perhaps not a set discriminator between carbonate and siliciclastic slope systems.

Another difference between siliciclastic and carbonate channels is the sinuosity and its relation to slope angle. In both siliciclastic (Clark et al. 1992) and carbonate channels, the sinuosity increases as the slope angle decreases. However, in comparison to sinuosity data from a siliciclastic system (Gee et al. 2007, Sylvester et al. 2013), the sinuosity of the channels in this study is far lower (Fig. 21). Gee et al. (2007) observed in siliciclastic channels that they evolve from straight, steeper channels to highly sinuous channels with lower channel-axis gradients. These channels start off as low-sinuosity channels that are largely confined by levees. Over time, the channel attempts to stabilize on the slope profile, and so they become more sinuous in order lower their channel-axis gradient. This process requires lateral accretion, which is not something that was often observed in the study area, which may explain why the sinuosity is so different.

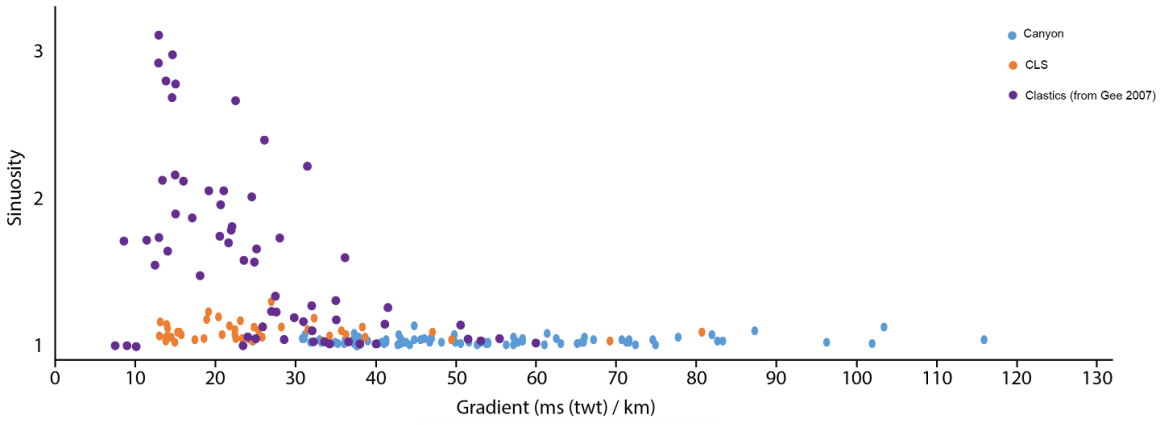

Figure 21: Comparison of sinuosity vs gradient between clastic submarine channels (adapted from Gee et al. 2017) and carbonate submarine canyons and channel levee systems.

Siliciclastic and classic carbonate slopes have vastly different gradients. The combination of high accommodation growth during periods of carbonate platform development and early diagenesis of carbonate sediment leads to the development of steeper slope gradients for carbonate systems (Schlager and Camber 1986, Playton et al. 2010). This is true for the slope of this study area as well, where the gradient is still much higher than the slope of a siliciclastic slope (Fig. 21). However, as mentioned previously, compared to the angles of other carbonate slopes, the slope of the study area is much less steep (2.4-11°), to the point of being more comparable to siliciclastic slope angles (3-6°, Playton et al. 2010) rather than the commonly referenced slope angles (30-45°, Janson et al. 2011, Playton et al. 2010).

Convergence and Divergence of Submarine Channels

Concavity of the shelf edge affects the convergence or divergence of channel-levee systems on the lower slope. Shelf edges with positive concavity can focus the sediment distribution into a downslope point source. This can significantly alter the geomorphologic

attributes of these channels, as the converging channels tend to be longer and slightly more sinuous than their non-convergent counterparts (Table 3). In this study, 2 areas of convergence show a convergence into a downdip channel or valley that extend outside the seismic survey. The slope angle of the lower slope on the convergent area seems to be steeper and of lower elevation. In contrast, the middle part of the study area has negative concavity and promote either divergent or parallel canyons and CLS. This is also the area where the slope fans developed. This area of the slope seems to have significantly more net sediment deposition than the more convergent area where more sediment bypass seems to occur. As a result, one can imagine these phenomena acting as a positive feedback where the negative concavity parts have more deposition, leading the lower angle promoting more deposition and promoting bulging outward of the slope. In contrast, positive concavity areas lead to convergent canyons and channels that seem to funnel the sediment further downslope, resulting in lower net deposition on the slope, a steeper initial angle, and more bypass. Potentially, the reentrant slope and convergence can ultimately lead to a major conduit for sediment far from the shelf edge and result in a large fan in the abyssal plain.

The Ocean Drilling Program (ODP) site 765A was drilled at the terminus of the southern reentrant of our survey. There the well encountered up to 350 m of Miocene calciturbidites. Because of the steep escarpment, this interval cannot be directly linked to the middle and lower slope in the 3D seismic survey but it illustrates how much sediment can bypass the entire slope system and accumulate on the abyssal plain. The fairly thick accumulation of calciturbidites in well 765A could be explained by the positive feedback between the shape of the slope and the amount of sediment exported basinward. Unfortunately, there is no other well to compare to in the region.

Topographical features on the slope can also have an effect on the sediment re-distribution downslope. In this study, long-lived positive features are created by large

MTDs. These slope-sourced MTDs not only erode and remobilize large volumes of the slope systems but also have a long-lasting effect on the down-slope sedimentation. The large slope collapse creates cohesive flows that tend to freeze and stop on the slope and create positive topography up to 85 m high (Fig. 15A). The topography created by the MTD then reroute subsequent submarine channels around them (Dennielou et al. 2019). Combined with a shelf edge with positive concavity, these MTD's can enhance the sediment focusing effect and the convergence of channel-levee systems on the lower slope. One example of this is featured in Curt 3 (Fig. 17), where the combination of a highly concave shelf edge and a large MTD forces multiple channels to merge into few combined channels that extends past the study area. Because these converged channels also receive more sediment than normal, they could exhibit traits more similar to that of point-sourced channels, including undergoing avulsion over time and having higher sinuosity (Gee et al. 2007).

CONCLUSION

Recent regional studies of carbonate shelf to slope systems have improved upon existing models, but fail to highlight the complexities of their slope architecture. This study of a high-resolution seismic volume attempts to quantify these complexities and adapt them into a new carbonate slope to toe-of-slope model.

Four distinct slope attributes were identified and quantified: channel-levee systems, canyons, MTDs, and fans. These attributes were distributed on the slope based on the slope gradient, with canyons occupying the upper slope (2.4-11°), the channel-levee systems occurring on the middle to lower slopes (1.2-4.6°), and the fans and MTDs in the lower slope (<3°).

Shelf edge concavity can play a major role in influencing downslope slope attributes, particularly the convergence of channel-levee systems. Shelf edges with positive concavity can force channel-levee systems to converge, while those with negative or negligible concavity usually do not. Converging channels tend to be longer and more sinuous, and almost all of them extended past boundaries of the study area. Non-converging channels were often terminated within the study area in the lower slope, and were usually accompanied by fans.

Topographical obstructions such MTDs can reroute nearby channel-levee systems. In conjunction with a shelf edge with a positive concavity, these obstructions can enhance the converging effects on channel-levee systems.

The sinuosities defined in this paper were significantly less than those gathered in studies of siliciclastic systems. The gradients of both canyons and channel-levee systems are higher, and the total channel lengths are much shorter. These factors are likely due to the different depositional settings and behaviors of carbonate and siliciclastic systems; the

carbonate deposits in this study area were sourced from carbonate buildups on the shelf, resulting in line-sourced channels, while siliciclastic deposits were point-sourced.

References

Adams, E.W. and Schlager, W., 2000. Basic types of submarine slope curvature. Journal of Sedimentary Research, 70(4), pp.814-828.

Apthorpe, M., 1988, Cainozoic depositional history of the North West Shelf, in Purcell, P.G., and Purcell, R.R., eds., The North West Shelf, Australia: Perth, Petroleum Exploration Society of Australia Symposium, Proceedings, pp.55–84.

Belde, J., Back, S., Bourget, J., and Reuning, L., 2017. Oligocene and Miocene Carbonate Platform Development in the Browse Basin, Australian Northwest Shelf. Journal of Sedimentary Research, 87(8), pp.795-816.

Bergantino, R.N., 1971. Submarine regional geomorphology of the Gulf of Mexico. Geological Society of America Bulletin, 82(3), pp.741-752.

Blevin, J.E., Struckmeyer, H.I.M., Cathro, D.L., Totterdell, J.M., Boreham, C.J., Romine, K.K., Loutit, T.S. and Sayers, J., 1998. Tectonostratigraphic framework and petroleum systems of the Browse Basin, North West Shelf. IN: Purcell, P.G. and Purcell, R.R. (Editors), The sedimentary basins of Western Australia 2: Proceedings of the Petroleum Exploration Society of Australia Symposium, Perth, 1998, 369-395.

Clark, J. D., Kenyon, N. H., & Pickering, K. T. (1992). Quantitative analysis of the geometry of submarine channels: implications for the classification of submarine fans. Geology, 20(7), pp.633-636.

Coniglio, M. and Dix, G.R., 1992. Chapter 18. Carbonate slopes. In: Facies models: Response to sea -level change (Ed. by R. G. Walter & N. P. James). Geological Association of Canada, 349 -374.

Collins, L.B., Read, J.F., Hogarth, J.W. and Coffey, B.P., 2006. Facies, outcrop gamma ray and C–O isotopic signature of exposed Miocene subtropical continental shelf carbonates, North West Cape, Western Australia. Sedimentary Geology, 185(1-2), pp.1-19.

Cook, H.E., Hine, A.C. and Mullins, H.T., 1983. Platform margin and deep water carbonates. Society of Economic Paleontologists and Mineralogists. SEPM Short Course (November 1983), v. 12, pp.573.

Counts, J.W., Jorry, S.J., Leroux, E., Miramontes, E., and Jouet, G., 2018. Sedimentation adjacent to atolls and volcano-cored carbonate platforms in the Mozambique Channel (SW Indian Ocean). Marine Geology, 404, pp.41-59.

Dennielou, B., Jégou, I., Droz, L., Jouet, G., Cattaneo, A., Berné, S., Aslanian, D., Loubrieu, B., Rabineau, M. and Bermell, S., 2019. Major modification of sediment routing by a large Mass Transport Deposit in the Gulf of Lions (Western Mediterranean). Marine Geology, 411, pp.1-20.

Ga.gov.au. 2020. Canning Basin | Geoscience Australia. [online] Available at: <https://www.ga.gov.au/scientific-topics/energy/province-sedimentary-basin-geology/petroleum/offshore-northwest-australia/canning> [Accessed 8 August 2020].

Gee, M.J.R., Gawthorpe, K., Bakke, K., Friedmann, and S.J., 2007. Seismic Geomorphology and Evolution of Submarine Channels from the Angolan Continental Margin. Journal of Sedimentary Research, 77, pp.433-446.

Hurd, G.S., Kerans, C., Fullmer, S. and Janson, X., 2016. Large-scale inflections in slope angle below the shelf break: A first order control on the stratigraphic architecture of carbonate slopes: Cutoff Formation, Guadalupe Mountains National Park, West Texas, USA. Journal of Sedimentary Research, 86(4), pp.336-362.

Janson, X., Kerans, C., Bellian, J.A., and Fitchen, W., 2007. Three-dimensional geological and synthetic seismic model of Early Permian redeposited basinal carbonate deposits, Victorio Canyon, west Texas. AAPG Bulletin, 91(10), pp.1405-1436.

Janson, X., Kerans, C., Loucks, R., Marhx, M.A., Reyes, C., and Murguia, F., 2011. Seismic architecture of a Lower Cretaceous platform-to-slope system, Santa Agueda and Poza Rica fields, Mexico. AAPG Bulletin 95(1), pp.105-146.

Kenter, J.A., 1990. Carbonate platform flanks: slope angle and sediment fabric. Sedimentology, 37(5), pp.777-794.

Kerans, C., Lucia, F.J, and Sengar, R.K., 1994. Integrated Characterization of Carbonate Ramp Reservoirs Using Permian San Andres Formation Outcrop Analogs. AAPG Bulletin, 78(2), pp.181-216.

Keep, M., Bishop, A., and Longley, I., 2000, Neogene wrench reactivation of the Barcoo Sub-basin, northwest Australia: implications for Neogene tectonics of the northern Australian margin: Petroleum Geoscience, 6, pp.211–220.

Marfurt, K.J., Kirlin, R.L., Farmer, S.L., and Bahorich, M.S., 1998. 3-D seismic attributes using a semblance-based coherency algorithm. Geophysics, 63(4), pp.1150-1165.

Mitchum Jr, R.M. and Vail, P.R., 1977. Seismic Stratigraphy and Global Changes of Sea Level: Part 7. Seismic Stratigraphic Interpretation Procedure: Section 2. Application of Seismic Reflection Configuration to Stratigraphic Interpretation, in C.E. Payton (ed.). Seismic Stratigraphy - Applications to Hydrocarbon Exploration: American Association of Petroleum Geologists Memoir 26, p. 135-143.

Mitchum Jr, R. M., Vail, P. R., & Sangree, J. B. (1977). Seismic stratigraphy and global changes of sea level: Part 6. Stratigraphic interpretation of seismic reflection patterns in depositional sequences: Section 2. Application of seismic reflection configuration to stratigraphic interpretation, in C.E. Payton (ed.). Seismic Stratigraphy - Applications to Hydrocarbon Exploration: American Association of Petroleum Geologists Memoir 26, p. 117-133.

Moss, G.D., Cathro, D.L. and Austin, J.A., 2004. Sequence biostratigraphy of prograding clinoforms, northern Carnarvon Basin, Western Australia: a proxy for variations in Oligocene to Pliocene global sea level? Palaios, 19(3), pp.206-226.

Mulder, T., Ducassou, E., Eberli, G.P., Hanquiez, V., Gonthier, E., Kindler, P., Principaud, M., Fournier, F., Léonide, P., Billeaud, I. and Marsset, B., 2012. New insights into the morphology and sedimentary processes along the western slope of Great Bahama Bank. Geology, 40(7), pp.603-606.

Mulder, T., Joumes, M., Hanquiez, V., Gillet, H., Reijmer, J.J.G., Tournadour, E., Chabaud, L., Principaud, M., Schnyder, J.S.D., Borgomano, J. and Fauquembergue, K., 2017. Carbonate slope morphology revealing sediment transfer from bank-to-slope (Little Bahama Bank, Bahamas). Marine and Petroleum Geology, 83, pp.26-34.

Mullins, H.T., and Cook, H.E., 1986. Carbonate apron models: Alternatives to the submarine fan model for paleoenvironmental analysis and hydrocarbon exploration. Sediment Geology, 48(1-2), pp.37-79.

Normark, W.R., Posamentier, H. and Mutti, E., 1993. Turbidite systems: state of the art and future directions. Reviews of Geophysics, 31(2), pp.91-116.

Partyka, G., Gridley, J., and Lopez, J., 1999. Interpretational Applications of Spectral Decomposition in Reservoir Characterization. The Leading Edge, 18, pp.353-360.

Paumard, V., Bourget, J., Payenberg, T., George, A.D., Ainsworth, R.B., and Lang, S., 2019. From quantitative 3D seismic stratigraphy to sequence stratigraphy: Insights into the vertical and lateral variability of shelf-margin depositional systems at different stratigraphic orders. Marine and Petroleum Geology, 110, pp.797-831.

Payros, A., and Pujalte, V., 2008. Calciclastic submarine fans: An integrated overview. Earth-Science Reviews, 86, pp.203-246.

Payros, A., Pujalte, V. and Orue=Etxebarria, X., 2007. A point-sourced calciclastic submarine fan complex (Eocene Anotz Formation, western Pyrenees): facies architecture, evolution and controlling factors. Sedimentology, 54(1), pp.137-168.

Phelps, R.M. and Kerans, C., 2007. Architectural characterization and three-dimensional modeling of a carbonate channel–levee complex: Permian San Andres Formation, Last Chance Canyon, New Mexico, USA. Journal of Sedimentary Research, 77(11), pp.939-964.

Piper, D. J., & Normark, W. R., 2001. Sandy fans-from Amazon to Hueneme and beyond. AAPG bulletin, 85(8), 1407-1438.

Playton, T.E., Janson, X., Kerans, C., 2010, Carbonate slopes in James, N.P. and Dalrymple, R.W. (eds), 2010. Facies models 4, Geological Association of Canada, 449 -476. pp.449-476.

Posamentier, H.W., and Kolla, V, 2003. Seismic Geomorphology and Stratigraphy of Depositional Elements in Deep-Water Settings. Journal of Sedimentary Research, 73(3), pp.367–388.

Posamentier, H.W., and Martinsen, O.J., 2010. The Character and Genesis of Submarine Mass-Transport Deposts: Insights from Outcrop and 3D Seismic Data. SEPM Special Publication, 95.

Principaud, M., Mulder, T., Gillet, H. and Borgomano, J., 2015. Large-scale carbonate submarine mass-wasting along the northwestern slope of the Great Bahama Bank (Bahamas): Morphology, architecture, and mechanisms. Sedimentary Geology, 317, pp.27-42.

Puga-Bernabéu, Á., Webster, J.M., Beaman, R.J. and Guilbaud, V., 2013. Variation in canyon morphology on the Great Barrier Reef margin, north-eastern Australia: The influence of slope and barrier reefs. Geomorphology, 191, pp.35-50.

Rosleff-Soerensen, B., Reuning, L., Back, S., and Kukla, P.A., 2012. Seismic geomorphology and growth architecture of a Miocene barrier reef, Browse Basin, NW-Australia. Marina and Petroleum Geology, 29 (1), pp.223-254.

Rosleff-Soerensen, B., Reuning, L., Back, S. and Kukla, P.A., 2016. The response of a basin-scale Miocene barrier reef system to long-term, strong subsidence on a passive continental margin, Barcoo Sub-basin, Australian North West Shelf. Basin Research, 28(1), pp.103-123.

Schlager, W. and Adams, E.W., 2001. Model for the sigmoidal curvature of submarine slopes. Geology, 29(10), pp.883-886.

Schlager, W., and Camber, O., 1986. Submarine slope angles, drowning unconformities, and self-erosion of limestone escarpments. Geology, 14(9), pp.762-765.

Sheridan, R.E., Crosby, J.T., Bryan, G.M. and Stoffa, P.L., 1981. Stratigraphy and structure of southern Blake Plateau, northern Florida Straits, and northern Bahama Platform from multichannel seismic reflection data. AAPG Bulletin, 65(12), pp.2571-2593.

Stephenson, A.E. and Cadman, S.J., 1994. Browse Basin, Northwest Australia: the evolution, palaeogeography and petroleum potential of a passive continental margin. Palaeogeography, Palaeoclimatology, Palaeoecology, 111(3-4), pp.337-366.

Struckmeyer, H.I.M., Blevin, J.E., Sayers, J., Totterdell, J.M., Baxter, K., and Cathro, D., 1998. Structural evolution of the Browse Basin, North West Shelf: new concepts from deep-seismic data. In: Purcell, P.G., Purcell, R.R. (Eds.), West Australia Basin Symposium, Perth, Western Australia.

Sylvester, Z., Pirmez, C., Cantelli, A., & Jobe, Z. R. (2013). Global (latitudinal) variation in submarine channel sinuosity: Comment. Geology, 41(5), e287-e287.

Tournadour, E., Mulder, T., Borgomano, J., Hanquiez, V., Ducassou, E. and Gillet, H., 2015. Origin and architecture of a mass transport complex on the northwest slope of Little Bahama Bank (Bahamas): relations between off-bank transport, bottom current sedimentation and submarine landslides. Sedimentary Geology, 317, pp.9-26.

Tuyl, J.V., Alves, T.M., and Cherns, L., 2018. Pinnacle features at the base of isolated carbonate buildups marking point sources of fluid offshore Northwest Australia. GSA Bulletin, 130 (9), pp.1596-1614.

Vail, P.R., R.M. Mitchum, Jr., and S. Thompson III, 1977, Seismic Stratigraphy and Global Changes of Sea Level: Part 3 - Relative Changes of Sea Level from Coastal Onlap, in C.E. Payton (ed.), Seismic Stratigraphy - Applications to Hydrocarbon Exploration: American Association of Petroleum Geologists Memoir 26, p. 63-81.

Veevers, J.J., and Cotteril, D., 1978. Western margin of Australia: evolution of a rifted arch system. GSA Bulletin, 89, pp.337-355.

Wood, L.J., 2007. Quantitative Seismic Geomorphology of Pliocene and Miocene Fluvial Systems in the Northern Gulf of Mexico, U.S.A. Journal of Sedimentary Research, 77(9), pp.713-730.